

An analysis of a new stable partitioned algorithm for FSI problems. Part I: Incompressible flow and elastic solids

J. W. Banks^{a,1}, W. D. Henshaw^{b,1,*}, D. W. Schwendeman^{b,2}

^a*Center for Applied Scientific Computing, Lawrence Livermore National Laboratory, Livermore, CA 94551, USA*

^b*Department of Mathematical Sciences, Rensselaer Polytechnic Institute, Troy, NY 12180, USA*

Abstract

Stable partitioned algorithms for fluid-structure interaction (FSI) problems are developed and analyzed in this two-part paper. Part I describes an algorithm for incompressible flow coupled with compressible elastic solids, while Part II discusses an algorithm for incompressible flow coupled with structural shells. Importantly, these new *added-mass partitioned* (AMP) schemes are stable and retain full accuracy with no sub-iterations per time step, even in the presence of strong added-mass effects (e.g. for light solids). The numerical approach described here for bulk compressible solids extends the scheme of Banks et al. [1, 2] for inviscid compressible flow, and uses Robin (mixed) boundary conditions with the fluid and solid solvers at the interface. The basic AMP Robin conditions, involving a linear combination of velocity and stress, are determined from the outgoing solid characteristic relation normal to the fluid-solid interface combined with the matching conditions on the velocity and traction. Two alternative forms of the AMP conditions are then derived depending on whether the fluid equations are advanced with a fractional-step method or not. The stability and accuracy of the AMP algorithm is evaluated for linearized FSI model problems; the full nonlinear case being left for future consideration. A normal mode analysis is performed to show that the new AMP algorithm is stable for any ratio of the solid and fluid densities, including the case of very light solids when added-mass effects are large. In contrast, it is shown that a traditional partitioned algorithm involving a Dirichlet-Neumann coupling for the same FSI problem is formally unconditionally unstable for any ratio of densities. Exact traveling wave solutions are derived for the FSI model problems, and these solutions are used to verify the stability and accuracy of the corresponding numerical results obtained from the AMP algorithm for the cases of light, medium and heavy solids.

Keywords: fluid-structure interaction, partitioned algorithms, added mass instability, incompressible fluid flow, elastic solids

*Department of Mathematical Sciences, Rensselaer Polytechnic Institute, 110 8th Street, Troy, NY 12180, USA.

Email addresses: banks20@llnl.gov (J. W. Banks), henshw@rpi.edu (W. D. Henshaw), schwed@rpi.edu (D. W. Schwendeman)

¹This work was performed under the auspices of the U.S. Department of Energy (DOE) by Lawrence Livermore National Laboratory under Contract DE-AC52-07NA27344 and by DOE contracts from the ASCR Applied Math Program.

²This research was supported by Lawrence Livermore National Laboratory under subcontract B548468, and by the National Science Foundation under grant DMS-1016188.

Contents

1	Introduction	3
2	Governing equations and interface conditions	5
3	Partitioned algorithms for FSI	7
4	FSI Model problems	10
5	An illustration of the AMP algorithm	11
6	Analysis of a two-dimensional acoustic solid and an inviscid incompressible fluid	13
6.1	Discretization	13
6.2	Stability analysis	15
6.3	AMP interface conditions	17
6.4	TP interface conditions	20
6.5	Anti-traditional interface conditions	20
7	The AMP FSI time-stepping algorithm	21
8	Numerical results	23
8.1	The method of analytic solutions	24
8.2	Traveling wave exact solutions	24
8.3	Traditional partitioned scheme	26
9	Conclusions	27
Appendix A	Traveling wave exact solutions for the FSI model problems	29
Appendix A.1	Traveling wave solution for MP-IA	30
Appendix A.2	Traveling wave solution for MP-VA	31
Appendix A.3	Traveling wave solution for MP-VE	32
Appendix B	AMP time-stepping procedures	32

1. Introduction

The coupled evolution of fluids and structures is of great interest in a wide range of applications including, for example, structural engineering and biomedicine. Such fluid-structure interaction (FSI) problems are often modeled mathematically by suitable partial differential equations for the fluids and structures in their respective domains, together with conditions at the boundaries of the domains where the solutions of the equations interact. Numerical algorithms used to solve these FSI problems can be classified into two main categories. Algorithms belonging to one category, called monolithic schemes, treat the equations for the domains of the fluids and structures along with interface conditions as a large system of evolution equations, and then advance the solutions together. The other category of algorithms are partitioned schemes (also known as modular or sequential schemes), and these algorithms employ separate solvers for the fluids and structures which are coupled at the interface. Typically, sub-iterations are performed at each time step of a partitioned algorithm for stability. Strongly-coupled partitioned schemes perform multiple iterations per time step to solve the coupled equations, while loosely coupled schemes use only one or a few iterations. Even though many existing partitioned schemes suffer from serious stability issues in certain problem regimes, they are often preferred since they can make use of existing solvers and can be more efficient than monolithic schemes.

In this paper we consider an important class of FSI problems where partitioned schemes often have difficulty. This class involves the coupling of incompressible fluids and relatively *light* structures where *added-mass* effects are large. Added-mass effects arise from the fact that the force required to accelerate a solid structure immersed in a fluid must also account for the acceleration of the surrounding fluid. Partitioned schemes for this class of problem generally suffer from poor convergence, requiring many sub-iterations per time step, or are unstable, when added-mass effects are large. The instabilities in partitioned schemes can be traced to the application of the interface conditions which must also be partitioned between the fluid and solid solvers. The traditional partitioned algorithm uses the velocity of the solid as a boundary condition on the fluid and the traction from the fluid as a forcing on the solid. This is sometimes referred to as Dirichlet-Neumann coupling with the Dirichlet condition being the assignment of the velocity and the Neumann condition the assignment of the traction. More generally, practitioners have considered Robin-Robin coupling (i.e. *mixed* boundary conditions for the fluid and solid) to impose the interface conditions [3].

The central aim of the present work is to describe an added-mass partitioned (AMP) algorithm for FSI problems involving an incompressible fluid coupled to an elastic structure. A key feature of our new AMP algorithm is that it is stable, even when added-mass effects are large, and it retains full accuracy with no sub-iterations. We discuss the algorithm and analyze its stability for two types of structures. In Part I of this paper, we describe the algorithm for FSI problems involving compressible bulk solids, while in Part II, we consider problems involving elastic shells. A common feature of the algorithms for both types of structures is the derivation of an AMP Robin interface condition for the fluid involving the velocity or acceleration of the interface and the stress on it. The version of the Robin interface condition involving the velocity, which applies for the bulk solid case only, may be used as a boundary condition for the partitioned solver for the fluid in velocity-divergence form. The version of the interface condition involving the acceleration applies for both cases, and can be used for the fluid solver in velocity-pressure form. In the latter case, a further manipulation of the Robin condition is carried out so that it provides a suitable boundary condition for the pressure in a fractional-step fluid solver. The details of the derivation of the AMP Robin condition depends on the type of structure, whether it be an elastic solid or an elastic shell, and this is principally where the discussion of the algorithms in the two parts of the paper, and the corresponding stability analyses and results, differ. For the case of a compressible bulk solid, the AMP interface condition is obtained based on characteristic equations for the solid applied at the interface, while for the case of the elastic shell, the interface condition is obtained from the evolution equation for the shell itself. This latter case is described in detail in Part II of the paper [4].

For the present work, we focus primarily on an analysis of the stability of the AMP algorithm, and therefore consider (linear) Stokes flow for the incompressible fluid coupled to a linearly elastic solid. Subsequent work will extend the AMP algorithm to fully nonlinear incompressible flow and elastic solids with large deformation, and will be based on the foundation laid in this paper. We introduce various two-dimensional model problems, each with a fluid-solid interface that is linearized about its initial position, and use these to study the behavior of the new algorithm and compare it with existing algorithms. A normal-mode analysis

of the algorithm applied to one of the model problems is used to show that the AMP algorithm is stable for any ratio of the fluid to solid densities, and in particular for the case of light solids where added-mass effects are large. In contrast, a stability analysis of a scheme based on the traditional Dirichlet-Neumann coupling is shown to be *formally* unconditionally unstable for any density ratio in the sense that the scheme may be stable on a coarse grid but becomes unstable for a sufficiently fine mesh³. The Stokes equations in our implementation of the AMP algorithm are solved with a fractional-step method based on a velocity-pressure formulation [6, 7] that can be made fully second-order (or higher-order) accurate. A key ingredient to this scheme is the proper specification of boundary conditions for the pressure. The elastic wave equation is solved with a second-order accurate upwind scheme for the equations written as a first-order system following the approach developed for overlapping grids in [8]. Together with the AMP interface condition, the partitioned algorithm is fully second-order accurate. The stability and accuracy is verified by comparing numerical solutions with exact traveling-wave solutions to three FSI model problems.

In previous work [2], a stable partitioned algorithm for *compressible* flows and compressible elastic solids was developed that overcomes the added-mass effect and uses deforming composite grids to treat large solid motions. FSI problems involving compressible flows are somewhat easier to deal with than incompressible flows since the added-mass effects are localized due to the finite speeds of wave propagation in the fluid [9]. The scheme in [2], which is based on the analysis in [1], uses a local characteristic analysis of a fluid-structure Riemann problem to define an impedance weighted averaging of the fluid and solid interface values (i.e. a Robin-Robin coupling). This algorithm was extended to the case of rigid bodies in [10] where it was shown that the scheme remains stable even for rigid bodies of zero mass.

The development and study of numerical algorithms for FSI problems is an active area of research, see for example, the papers [11–18] and the references cited therein. In particular, there has been much work concerning partitioned algorithms and the added-mass effect. For the case of incompressible fluids coupled to thin structural shells, there has been some success in treating the added-mass instability. The kinematically-coupled scheme of Guidoboni et al. [19], later extended to the β -scheme by Čanić, Muha and Bukač [20], is a stable partitioned scheme that uses operator splitting. Nobile and Vergara [21], among others, have developed stable semi-monolithic schemes for the case of thin shells. Even fully monolithic schemes for thin-shells [22] are not overly expensive since the number of degrees of freedom for the structural shell is usually small compared to those in the fluid. For bulk solids, however, apparently all previous partitioned approaches for coupling incompressible flows and light solids are either unstable or require multiple sub-iterations per time step to converge (tens or hundreds of iterations are typical) with the number of iterations generally increasing as the solid gets lighter. Indeed, it is common to resort to fully monolithic schemes [13, 23–25] or semi-monolithic schemes [17, 26, 27].

A number of authors have analyzed the added-mass effect and the stability of FSI algorithms [9, 27–32]. Causin, Gerbeau and Nobile [33], for example, analyze a model problem of a structural shell coupled to an incompressible fluid and show that the traditional scheme can be unconditionally unstable over a certain range of parameters. There are numerous approaches that have been developed to reduce the number of iterations required per time step in partitioned schemes [30]. Robin-Robin interface conditions are used to stabilize partitioned schemes by, for example, Nobile, Vergara and co-workers [3, 21, 32, 34, 35] and Astorino, Chouly and Fernandez [27]. Yu, Baek and Karniadakis [36] and Baek and Karniadakis [37] have developed fictitious-pressure and fictitious-mass algorithms which incorporate additional terms into the governing equations to account for added-mass effects. The optimal values for parameters are estimated from analysis and computation, and the number of sub-iterations required using Aitken acceleration (tens of iterations) is similar to optimal Robin-Robin approaches. To stabilize the FSI algorithm and reduce the number of sub-iterations, Riemsdagh, Vierendeels and Dick [38], Degroote et al. [39], and Raback, Ruokolainen, and Lyly [40] have developed an interface artificial compressibility method that adds a source term to the fluid continuity equation near the interface; the effect of the source term goes away as the sub-iterations converge. Idelsohn et al. [41] and Badia, Quaini and Quarteroni [42] form approximate factorizations of the fully monolithic scheme to construct partitioned schemes but these still may require many iterations to converge. Degroote

³Formally, a scheme is said to be stable, if for a given time interval, the numerical solutions can be bounded, independent of the mesh spacing, for all mesh spacings sufficiently small [5]. We will sometimes informally refer to a scheme being stable for some particular values of the mesh spacing and time step.

et al. [43, 44] use reduced-order models and Aitken acceleration methods to decrease the number of iterations in partitioned schemes.

The remainder of the manuscript is organized as follows. In Section 2 we define the governing equations and present the essential form of the AMP interface conditions. In Section 3 there is a discussion of partitioned algorithms and how the AMP interface conditions are incorporated into the fluid and solid solution schemes. Three model problems are defined in Section 4 and these are used later for the analysis and numerical results. In Section 5 the form of the AMP algorithm for a one-dimensional model problem is discussed. A normal mode stability analysis of the AMP scheme as well as the traditional (Dirichlet-Neumann) and anti-traditional (Neumann-Dirichlet) schemes are presented in Section 6. The FSI time-stepping algorithm for the AMP scheme is outlined in Section 7. Section 8 provides numerical results confirming the stability and accuracy of the scheme. Conclusions are given in Section 9. A summary comparison of the algorithm discussed here for bulk solids with the one for structural shells is provided at the end of Part II of this paper [4].

2. Governing equations and interface conditions

We consider a fluid-structure interaction problem in which an incompressible fluid in a domain Ω^F is coupled to a compressible elastic solid in a domain Ω^S . The interface where the two domains meet is assumed to be smooth and is denoted by Γ . For the purposes of this paper, we consider an FSI problem consisting of small perturbations about an equilibrium state. Thus, we assume that the nonlinear convection terms in the fluid are negligible and the solid is linearly elastic, and we consider the problem to be linearized about a fixed interface position. We also neglect the effects of gravity or other body forces. Under these assumptions, the flow in the fluid domain is governed by the linear Stokes equations

$$\rho \frac{\partial \mathbf{v}}{\partial t} = \nabla \cdot \boldsymbol{\sigma}, \quad \mathbf{x} \in \Omega^F, \quad (1)$$

$$\nabla \cdot \mathbf{v} = 0, \quad \mathbf{x} \in \Omega^F, \quad (2)$$

where \mathbf{x} is position, t is time, ρ is the (constant) fluid density, and $\mathbf{v} = \mathbf{v}(\mathbf{x}, t)$ is the fluid velocity. In the linearized approximation, the Eulerian fluid domain Ω^F does not deform and remains fixed in time. The fluid stress tensor, $\boldsymbol{\sigma} = \boldsymbol{\sigma}(\mathbf{x}, t)$, is given by

$$\boldsymbol{\sigma} = -p\mathbf{I} + \boldsymbol{\tau}, \quad \boldsymbol{\tau} = \mu [\nabla \mathbf{v} + (\nabla \mathbf{v})^T], \quad (3)$$

where p is the pressure, \mathbf{I} is the identity tensor, $\boldsymbol{\tau}$ is the viscous stress tensor, and μ is the (constant) fluid viscosity. For future reference, the components of a vector, such as \mathbf{v} will be denoted by v_m , $m = 1, 2, 3$, (i.e. $\mathbf{v} = [v_1, v_2, v_3]^T$), while components of a tensor such as $\boldsymbol{\sigma}$, will be denoted by σ_{mn} , $m, n = 1, 2, 3$. In the solid domain, the solid displacement $\bar{\mathbf{u}} = \bar{\mathbf{u}}(\mathbf{x}, t)$ and velocity $\bar{\mathbf{v}} = \bar{\mathbf{v}}(\mathbf{x}, t)$ are governed by

$$\frac{\partial \bar{\mathbf{u}}}{\partial t} = \bar{\mathbf{v}}, \quad \mathbf{x} \in \Omega^S, \quad (4)$$

$$\bar{\rho} \frac{\partial \bar{\mathbf{v}}}{\partial t} = \nabla \cdot \bar{\boldsymbol{\sigma}}, \quad \mathbf{x} \in \Omega^S, \quad (5)$$

where $\bar{\rho}$ is the (constant) solid density and $\bar{\boldsymbol{\sigma}} = \bar{\boldsymbol{\sigma}}(\mathbf{x}, t)$ is the Cauchy stress tensor⁴. In the linearized approximation, the Lagrangian reference coordinates for the solid are the same as the Eulerian coordinates \mathbf{x} . The stress tensor is given by

$$\bar{\boldsymbol{\sigma}} = \bar{\lambda}(\nabla \cdot \bar{\mathbf{u}})\mathbf{I} + \bar{\mu} [\nabla \bar{\mathbf{u}} + \nabla \bar{\mathbf{u}}^T],$$

where $\bar{\lambda}$ and $\bar{\mu}$ are (constant) Lamé parameters. The matching conditions at the fluid-solid interface Γ are

$$\mathbf{v}(\mathbf{x}, t) = \bar{\mathbf{v}}(\mathbf{x}, t), \quad \mathbf{x} \in \Gamma, \quad (6)$$

$$\boldsymbol{\sigma}(\mathbf{x}, t)\mathbf{n} = \bar{\boldsymbol{\sigma}}(\mathbf{x}, t)\mathbf{n}, \quad \mathbf{x} \in \Gamma, \quad (7)$$

⁴ Over-bars on symbols are used throughout the paper to denote quantities belonging to the solid.

where \mathbf{n} is the outward unit normal to the fluid domain. The problem is closed by specifying initial conditions for \mathbf{v} in Ω^F and for $\bar{\mathbf{u}}$ and $\bar{\mathbf{v}}$ in Ω^S , and by specifying suitable conditions on the boundaries of the fluid and solid domains not included in Γ .

The elastic wave equations in (4) and (5) form a hyperbolic system with a characteristic structure and finite wave speeds. These wave speeds, given by

$$\bar{c}_p = \sqrt{\frac{\bar{\lambda} + 2\bar{\mu}}{\bar{\rho}}}, \quad \bar{c}_s = \sqrt{\frac{\bar{\mu}}{\bar{\rho}}},$$

are the propagation speeds of p-waves and s-waves, respectively, in the elastic solid. At the interface the equations can be locally transformed into normal and tangential coordinates. By considering the components of the equations in the normal direction, one can define characteristics and characteristic variables [45] that indicate the propagation of information in the direction normal to the interface. The *incoming* and *outgoing* characteristic variables normal to the interface are given by

$$\mathcal{A}(\bar{\boldsymbol{\sigma}}, \bar{\mathbf{v}}) = \mathbf{n}^T \bar{\boldsymbol{\sigma}} \mathbf{n} - \bar{z}_p \mathbf{n}^T \bar{\mathbf{v}}, \quad \mathbf{x} \in \Gamma \quad (\text{incoming}), \quad (8)$$

$$\mathcal{A}_m(\bar{\boldsymbol{\sigma}}, \bar{\mathbf{v}}) = \mathbf{e}_m^T \bar{\boldsymbol{\sigma}} \mathbf{n} - \bar{z}_s \mathbf{e}_m^T \bar{\mathbf{v}}, \quad m = 1, 2, \quad \mathbf{x} \in \Gamma \quad (\text{incoming}), \quad (9)$$

$$\mathcal{B}(\bar{\boldsymbol{\sigma}}, \bar{\mathbf{v}}) = \mathbf{n}^T \bar{\boldsymbol{\sigma}} \mathbf{n} + \bar{z}_p \mathbf{n}^T \bar{\mathbf{v}}, \quad \mathbf{x} \in \Gamma \quad (\text{outgoing}), \quad (10)$$

$$\mathcal{B}_m(\bar{\boldsymbol{\sigma}}, \bar{\mathbf{v}}) = \mathbf{e}_m^T \bar{\boldsymbol{\sigma}} \mathbf{n} + \bar{z}_s \mathbf{e}_m^T \bar{\mathbf{v}}, \quad m = 1, 2, \quad \mathbf{x} \in \Gamma \quad (\text{outgoing}). \quad (11)$$

Here, $\bar{z}_p = \bar{\rho} \bar{c}_p$ and $\bar{z}_s = \bar{\rho} \bar{c}_s$ are the solid impedances for p-waves and s-waves, respectively, and \mathbf{e}_m , $m = 1, 2$ denote mutually orthogonal unit vectors tangent to the interface. By *outgoing* we mean the characteristics that leave the solid domain through the interface, and vice versa for the *incoming* characteristics.

Partitioned algorithms impose the interface conditions (6) and (7) by defining segregated conditions for the fluid and solid domains. In the traditional partitioned algorithm, the interface condition in (6) is taken to be the (Dirichlet) boundary condition for the fluid (velocity from solid), while (7) is taken to be the (Neumann) boundary condition for the solid (traction from fluid). Alternatively, the approach we develop in this article is based on using the incoming and outgoing solid characteristic variables normal to the interface given in (8)–(11). In this approach a Robin interface condition for the fluid is defined in terms of the outgoing solid characteristic variables, namely

$$\mathcal{B}(\boldsymbol{\sigma}, \mathbf{v}) = \mathcal{B}(\bar{\boldsymbol{\sigma}}, \bar{\mathbf{v}}), \quad \mathcal{B}_m(\boldsymbol{\sigma}, \mathbf{v}) = \mathcal{B}_m(\bar{\boldsymbol{\sigma}}, \bar{\mathbf{v}}), \quad m = 1, 2, \quad \mathbf{x} \in \Gamma, \quad (12)$$

while a Robin interface condition for the solid is defined in terms of the fluid variables using the incoming characteristic variables

$$\mathcal{A}(\bar{\boldsymbol{\sigma}}, \bar{\mathbf{v}}) = \mathcal{A}(\boldsymbol{\sigma}, \mathbf{v}), \quad \mathcal{A}_m(\bar{\boldsymbol{\sigma}}, \bar{\mathbf{v}}) = \mathcal{A}_m(\boldsymbol{\sigma}, \mathbf{v}), \quad m = 1, 2, \quad \mathbf{x} \in \Gamma. \quad (13)$$

This, in a nutshell, is the key ingredient of the added-mass partitioned (AMP) algorithm. These conditions are linearly independent combinations of the interface conditions in (6) and (7), and are thus equivalent to the original conditions.

In practice, numerical computations, including those presented in Section 8, are often based on alternative forms of the governing equations. For the case of the fluid, the equations may be written in the velocity-pressure form

$$\rho \frac{\partial \mathbf{v}}{\partial t} + \nabla p = \mu \Delta \mathbf{v}, \quad \mathbf{x} \in \Omega^F, \quad (14)$$

$$\Delta p = 0, \quad \mathbf{x} \in \Omega^F. \quad (15)$$

We use a numerical approximation of this form of the equations to advance the fluid variables following the fractional-step method described in [6]. As discussed in [6], an additional boundary condition is required for this form of the equations, and a suitable choice is given by

$$\nabla \cdot \mathbf{v} = 0, \quad \mathbf{x} \in \partial\Omega^F. \quad (16)$$

For the solid domain, we consider the equations of linear elasticity written as the first-order system

$$\frac{\partial \bar{\mathbf{u}}}{\partial t} = \bar{\mathbf{v}}, \quad \mathbf{x} \in \Omega^S, \quad (17)$$

$$\bar{\rho} \frac{\partial \bar{\mathbf{v}}}{\partial t} = \nabla \cdot \bar{\boldsymbol{\sigma}}, \quad \mathbf{x} \in \Omega^S, \quad (18)$$

$$\frac{\partial \bar{\boldsymbol{\sigma}}}{\partial t} = \bar{\lambda}(\nabla \cdot \bar{\mathbf{v}})\mathbf{I} + \bar{\mu}[\nabla \bar{\mathbf{v}} + \nabla \bar{\mathbf{v}}^T], \quad \mathbf{x} \in \Omega^S, \quad (19)$$

and use a numerical approximation of this form of the equations to advance the solid variables following the second-order upwind (Godunov) method discussed in [8].

3. Partitioned algorithms for FSI

In this section we describe a traditional partitioned (TP) algorithm and compare it to our new *added-mass* partitioned (AMP) algorithm. For both algorithms, we assume that the discrete solution of the FSI problem is known at time t^{n-1} with fluid state $\mathbf{q}^{n-1} = (\mathbf{v}_i^{n-1}, p_i^{n-1}, \boldsymbol{\sigma}_i^{n-1})$ and solid state $\bar{\mathbf{q}}^{n-1} = (\bar{\mathbf{u}}_i^{n-1}, \bar{\mathbf{v}}_i^{n-1}, \bar{\boldsymbol{\sigma}}_i^{n-1})$ on a grid with mesh points \mathbf{x}_i . The algorithms then describe how to obtain the solutions \mathbf{q}^n and $\bar{\mathbf{q}}^n$ at a time $t^n = t^{n-1} + \Delta t$, where Δt is a chosen time step. For accuracy or stability reasons, multiple sub-iterations per time step may be needed in the TP algorithm [9], and we let $\mathbf{q}^{(k)}$ and $\bar{\mathbf{q}}^{(k)}$ denote the k^{th} iterates which are approximations of \mathbf{q}^n and $\bar{\mathbf{q}}^n$, respectively. The AMP algorithm, in contrast, requires no sub-iterations, and remains stable even for problems where added-mass effects are significant. Although not required, in practice we generally use a predictor-corrector algorithm, with a single correction step, to advance the fluid since it has a larger stability region that includes the imaginary axis [6]. We let $\mathbf{q}^{(p)}$ and $\bar{\mathbf{q}}^{(p)}$ denote solutions at the predictor step.

We begin with a discussion of a TP algorithm that is typical of the traditional algorithm used in practice. In this traditional FSI algorithm, the interface conditions in (6) and (7) are assigned separately in the two main steps, either the step to advance the solid or the step to advance the fluid. In particular, the velocity interface condition in (6) is associated with the fluid domain so that, from the point of view of the fluid, the interface is thought of as a no-slip moving wall. The traction condition in (7), on the other hand, is associated with the solid domain so that, from the solid's point of view, the interface is thought of as a no-slip traction wall.

TP Algorithm (traditional partitioned).

1. Choose some initial guess, e.g., $\mathbf{q}^{(0)} = \mathbf{q}^{n-1}$, $\bar{\mathbf{q}}^{(0)} = \bar{\mathbf{q}}^{n-1}$, and set $k = 1$.
2. Solve for $\bar{\mathbf{q}}^{(k)}$ in the solid domain using the traction boundary condition $(\bar{\boldsymbol{\sigma}}\mathbf{n})^{(k)} = (\boldsymbol{\sigma}\mathbf{n})^{(k-1)}$ on the interface.
3. Solve for $\mathbf{q}^{(k)}$ in the fluid domain using the velocity boundary condition $\mathbf{v}^{(k)} = \bar{\mathbf{v}}^{(k)}$ on the interface.
4. Set $k \leftarrow k + 1$ and iterate steps 2–4, as needed.

The TP algorithm given above may be unstable or require many under-relaxed sub-iterations per time step to converge when the added-mass effects are large (the *light* solid case). In fact, we show later that this scheme can be unconditionally unstable no matter how heavy the solid is in comparison to the fluid.

The AMP algorithm, which requires no sub-iterations, uses a different construction of the interface conditions obtained from the characteristic-based Robin (mixed) boundary conditions. The AMP algorithm outlined below contains the essential ingredients of the algorithm we use in practice. It uses a single stage predictor; one can optionally include a correction step if desired. More details are provided in subsequent discussions and in Section 7.

AMP Algorithm (added-mass partitioned).

1. Advance the solution in the solid domain to obtain $\bar{\mathbf{q}}^{(p)}$, and compute predicted values of the outgoing characteristic variables, $\mathcal{B}(\bar{\boldsymbol{\sigma}}^{(p)}, \bar{\mathbf{v}}^{(p)})$ and $\mathcal{B}_m(\bar{\boldsymbol{\sigma}}^{(p)}, \bar{\mathbf{v}}^{(p)})$, $m = 1, 2$.
2. Advance the solution in the fluid domain to obtain $\mathbf{q}^{(p)}$ using the boundary conditions $\mathcal{B}(\boldsymbol{\sigma}^{(p)}, \mathbf{v}^{(p)}) = \mathcal{B}(\bar{\boldsymbol{\sigma}}^{(p)}, \bar{\mathbf{v}}^{(p)})$ and $\mathcal{B}_m(\boldsymbol{\sigma}^{(p)}, \mathbf{v}^{(p)}) = \mathcal{B}_m(\bar{\boldsymbol{\sigma}}^{(p)}, \bar{\mathbf{v}}^{(p)})$, $m = 1, 2$, obtained from (12).

3. Define the interface traction $(\boldsymbol{\sigma}\mathbf{n})^I$ to be the traction at the interface of the fluid domain, and compute an interface velocity \mathbf{v}^I using an impedance weighted average of the velocities at the interface of the fluid and solid domain (as is defined later).
4. Apply solid interface conditions on $\bar{\mathbf{q}}^{(p)}$ using \mathbf{v}^I and $(\boldsymbol{\sigma}\mathbf{n})^I$.
5. Set $\mathbf{q}^n = \mathbf{q}^{(p)}$ and $\bar{\mathbf{q}}^n = \bar{\mathbf{q}}^{(p)}$.

Having outlined the basic steps of the two FSI algorithms, we now provide some further details of the new AMP algorithm. In Step 1 of the AMP algorithm, the discrete solution in the solid domain is advanced a time step Δt . This can be done, for example, using an approximation of the first-order system in (17)–(19) as described in [8]. Advancing the discrete solution in the fluid domain, as given in Step 2, may be done, for example, using the velocity-divergence form of the equations in (1) and (2) along with conditions on the interface given by

$$-p + \mathbf{n}^T \boldsymbol{\tau} \mathbf{n} + \bar{z}_p \mathbf{n}^T \mathbf{v} = \mathcal{B}(\bar{\boldsymbol{\sigma}}^{(p)}, \bar{\mathbf{v}}^{(p)}), \quad \mathbf{x} \in \Gamma, \quad (20)$$

$$\mathbf{e}_m^T \boldsymbol{\tau} \mathbf{n} + \bar{z}_s \mathbf{e}_m^T \mathbf{v} = \mathcal{B}_m(\bar{\boldsymbol{\sigma}}^{(p)}, \bar{\mathbf{v}}^{(p)}), \quad m = 1, 2, \quad \mathbf{x} \in \Gamma, \quad (21)$$

(and some boundary conditions for $\mathbf{x} \in \partial\Omega^F \setminus \Gamma$ which we do not discuss). We have used (3) to eliminate $\boldsymbol{\sigma}$ in (20) and (21) to reveal the dependence on the pressure p and the viscous stress $\boldsymbol{\tau} = \mu [\nabla \mathbf{v} + (\nabla \mathbf{v})^T]$. This shows that (20) involves both p and \mathbf{v} while (21) only depends on \mathbf{v} .

We prefer to advance the discrete solution in the fluid domain (for Step 2) using a fractional-step method based on the velocity-pressure form of the equations given in (14) and (15). In this approach, the velocity and pressure are advanced in separate stages. The two conditions at the interface given by (21), with $m = 1, 2$, along with the divergence condition in (16) provide suitable conditions for the numerical integration of (14) to advance the velocity. For the numerical solution of the Poisson problem for pressure in (15) we use a boundary condition based on an alternate version of the interface condition in (20). To motivate this condition, we first consider the linear Taylor approximation

$$\mathbf{v}(\mathbf{x}, t - \Delta t) \approx \mathbf{v}(\mathbf{x}, t) - \Delta t \frac{\partial \mathbf{v}}{\partial t}(\mathbf{x}, t)$$

and a similar approximation for the solid velocity. These Taylor approximations are used in (20) to obtain

$$\mathbf{n}^T \boldsymbol{\sigma} \mathbf{n} + \bar{z}_p \Delta t \mathbf{n}^T \frac{\partial \mathbf{v}}{\partial t} = \mathbf{n}^T \bar{\boldsymbol{\sigma}} \mathbf{n} + \bar{z}_p \Delta t \mathbf{n}^T \frac{\partial \bar{\mathbf{v}}}{\partial t}, \quad \mathbf{x} \in \Gamma, \quad (22)$$

assuming that $\mathbf{v}(\mathbf{x}, t - \Delta t) = \bar{\mathbf{v}}(\mathbf{x}, t - \Delta t)$ for $\mathbf{x} \in \Gamma$ according to (6). Note that even though a first-order accurate Taylor approximation was used in deriving (22), the condition is actually identically true since it is a linear combination of (7) and the time derivative of (6). Eliminating $\partial \mathbf{v} / \partial t$ in (22) using the fluid momentum equation (14) gives

$$-p - \frac{\bar{z}_p \Delta t}{\rho} \frac{\partial p}{\partial n} + \mathbf{n}^T \boldsymbol{\tau} \mathbf{n} - \frac{\mu \bar{z}_p \Delta t}{\rho} \mathbf{n}^T (\nabla \times \nabla \times \mathbf{v}) = \mathbf{n}^T \bar{\boldsymbol{\sigma}} \mathbf{n} + \bar{z}_p \Delta t \mathbf{n}^T \frac{\partial \bar{\mathbf{v}}}{\partial t}, \quad \mathbf{x} \in \Gamma. \quad (23)$$

The condition in (23) forms a suitable Robin condition for pressure and is the key ingredient of the AMP algorithm for fractional step fluid solvers. Note that the Robin condition only depends on \mathbf{v} through the viscous traction and diffusion operator, which generally makes (23) a better boundary condition to use when solving the pressure equation separately. We have also made the substitution $\Delta \mathbf{v} = -\nabla \times \nabla \times \mathbf{v}$, valid when $\nabla \cdot \mathbf{v} = 0$, since this improves the stability of implicit time-stepping schemes [7].

The discussion of our fractional-step scheme to advance the solution in the fluid domain for Step 2 may be summarized by defining the following two fluid sub-problems:

Velocity sub-problem. Assuming a known solution in the fluid domain at time $t - \Delta t$ and a predicted solution in the solid domain at time t , a discrete solution to the velocity at time t is determined by solving an appropriate discretization of

$$\rho \frac{\partial \mathbf{v}}{\partial t} - \mu \Delta \mathbf{v} = -\nabla p, \quad \mathbf{x} \in \Omega^F, \quad (24)$$

with boundary conditions

$$\begin{aligned} \mathbf{e}_m^T \mathbf{v} + \frac{1}{\bar{z}_s} \mathbf{e}_m^T \boldsymbol{\tau} \mathbf{n} &= \mathbf{e}_m^T \bar{\mathbf{v}} + \frac{1}{\bar{z}_s} \mathbf{e}_m^T \bar{\boldsymbol{\sigma}} \mathbf{n}, & m = 1, 2, & \quad \mathbf{x} \in \Gamma, \\ \nabla \cdot \mathbf{v} &= 0, & & \quad \mathbf{x} \in \Gamma, \end{aligned} \quad (25)$$

along with suitable boundary conditions for $\mathbf{x} \in \partial\Omega^F \setminus \Gamma$.

Pressure sub-problem. Given the discrete solution for \mathbf{v} at time t from the velocity sub-problem, the pressure is found using a discrete form of

$$\Delta p = 0, \quad \mathbf{x} \in \Omega^F,$$

with the Robin boundary condition

$$-p - \frac{\bar{z}_p \Delta t}{\rho} \frac{\partial p}{\partial n} = -\mathbf{n}^T \boldsymbol{\tau} \mathbf{n} + \frac{\mu \bar{z}_p \Delta t}{\rho} \mathbf{n}^T (\nabla \times \nabla \times \mathbf{v}) + \mathbf{n}^T \bar{\boldsymbol{\sigma}} \mathbf{n} + \bar{z}_p \Delta t \mathbf{n}^T \frac{\partial \bar{\mathbf{v}}}{\partial t}, \quad \mathbf{x} \in \Gamma, \quad (26)$$

and suitable boundary conditions for $\mathbf{x} \in \partial\Omega^F \setminus \Gamma$.

Moving on to Step 3 in the AMP algorithm, the interface traction, denoted by $(\boldsymbol{\sigma} \mathbf{n})^I$, is defined to be that from the fluid at time t ,

$$(\boldsymbol{\sigma} \mathbf{n})^I = -p \mathbf{n} + \boldsymbol{\tau} \mathbf{n}, \quad \mathbf{x} \in \Gamma, \quad (27)$$

since the fluid velocity and pressure have already incorporated the primary AMP interface conditions. The interface velocity, denoted by \mathbf{v}^I , can be defined directly from the fluid velocity as determined by the solution of the velocity sub-problem on $\mathbf{x} \in \Gamma$, or it can be defined by the fluid velocity \mathbf{v} as determined from characteristic relations in (12), which may be written in the form

$$\mathbf{n}^T \mathbf{v} = \mathbf{n}^T \bar{\mathbf{v}} + \frac{1}{\bar{z}_p} \mathbf{n}^T (\bar{\boldsymbol{\sigma}} \mathbf{n} - (\boldsymbol{\sigma} \mathbf{n})^I), \quad \mathbf{x} \in \Gamma, \quad (28)$$

$$\mathbf{e}_m^T \mathbf{v} = \mathbf{e}_m^T \bar{\mathbf{v}} + \frac{1}{\bar{z}_s} \mathbf{e}_m^T (\bar{\boldsymbol{\sigma}} \mathbf{n} - (\boldsymbol{\sigma} \mathbf{n})^I), \quad m = 1, 2, \quad \mathbf{x} \in \Gamma. \quad (29)$$

The analysis in Section 6 leading to Theorem 1 shows that these two choices are equivalent, at least for the one-dimensional approximation that was analyzed. However, the choice given by (28) and (29) is the better conditioned approximation for the case of *heavy* solids, while defining \mathbf{v}^I directly from the fluid velocity is better for *light* solids. To smoothly accommodate both limits, we define the interface velocity as an impedance-weighted average of the two choices, namely

$$\mathbf{n}^T \mathbf{v}^I = \frac{z_f}{z_f + \bar{z}_p} \mathbf{n}^T \mathbf{v} + \frac{\bar{z}_p}{z_f + \bar{z}_p} \mathbf{n}^T \bar{\mathbf{v}} + \frac{1}{z_f + \bar{z}_p} \mathbf{n}^T (\bar{\boldsymbol{\sigma}} \mathbf{n} - (\boldsymbol{\sigma} \mathbf{n})^I), \quad \mathbf{x} \in \Gamma, \quad (30)$$

$$\mathbf{e}_m^T \mathbf{v}^I = \frac{z_f}{z_f + \bar{z}_s} \mathbf{e}_m^T \mathbf{v}^f + \frac{\bar{z}_s}{z_f + \bar{z}_s} \mathbf{t}_m^T \bar{\mathbf{v}} + \frac{1}{z_f + \bar{z}_s} \mathbf{t}_m^T (\bar{\boldsymbol{\sigma}} \mathbf{n} - (\boldsymbol{\sigma} \mathbf{n})^I), \quad m = 1, 2, \quad \mathbf{x} \in \Gamma. \quad (31)$$

Here, $z_f = \rho v_f$ is the fluid impedance, where v_f is some suitable measure of the velocity in the fluid, such as the choice that naturally appears in the one-dimensional analysis of Section 5. Note that in practice, the algorithm is found to be very insensitive to the particular choice of v_f . This insensitivity is also confirmed in the theoretical results in Section 6. Also note the form of the impedance weighted averaged in (30) and (31) are the same form as those appearing in the added-mass algorithm for compressible fluids [2]. Finally, the interface values \mathbf{v}^I and $(\boldsymbol{\sigma} \mathbf{n})^I$ are used to assign boundary conditions on the solid in Step 4 of the AMP algorithm.

4. FSI Model problems

Three FSI model problems, of increasing complexity, are now defined. Model problem MP-IA, for an inviscid incompressible fluid and *acoustic* solid (defined below), is used in the two-dimensional analysis of partitioned schemes in Section 6, as well as being the basis for the one-dimensional model problem discussed in Section 5. The second model problem, MP-VA, includes the effects of viscosity in the fluid but retains the acoustic solid. Model problem MP-VE includes viscosity in the fluid and treats a linearly elastic solid. Exact traveling wave solutions to these model problems are given in Appendix A, while numerical simulations are given in Section 8. In all cases the fluid domain is the rectangular region $\Omega^F = (0, L) \times (-H, 0)$, the solid domain is $\Omega^S = (0, L) \times (0, \bar{H})$ and the interface is $\Gamma = \{(x, y) \mid x \in (0, L), y = 0\}$, see Figure 1. We consider solutions that are periodic in the x direction with period L .

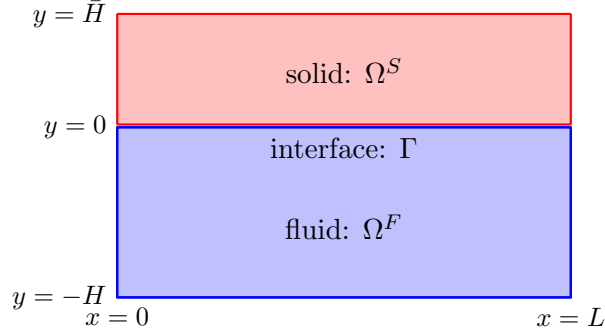


Figure 1: The geometry for the 2D FSI model problems.

Model Problem MP-IA. *Model problem MP-IA defines an inviscid incompressible fluid and an “acoustic” solid, that only supports vertical motion,*

$$\begin{aligned}
 \text{Fluid: } & \begin{cases} \rho \frac{\partial \mathbf{v}}{\partial t} + \nabla p = 0, & \mathbf{x} \in \Omega^F, \\ \nabla \cdot \mathbf{v} = 0, & \mathbf{x} \in \Omega^F, \\ v_2(x, -H, t) = 0 \text{ or } p(x, -H, t) = 0, \end{cases} & \text{Solid: } & \begin{cases} \bar{\rho} \frac{\partial^2 \bar{u}_2}{\partial t^2} = \bar{\rho} \bar{c}_p^2 \Delta \bar{u}_2, & \mathbf{x} \in \Omega^S, \\ u_2(x, \bar{H}, t) = 0, \end{cases} & (32) \\
 \text{Interface: } & v_2 = \frac{\partial \bar{u}_2}{\partial t}, \quad -p = \bar{\rho} \bar{c}_p^2 \frac{\partial \bar{u}_2}{\partial y}, \quad \mathbf{x} \in \Gamma.
 \end{aligned}$$

Model Problem MP-VA. *Model problem MP-VA defines a viscous incompressible fluid and an “acoustic” solid, that only supports vertical motion,*

$$\begin{aligned}
 \text{Fluid: } & \begin{cases} \rho \frac{\partial \mathbf{v}}{\partial t} + \nabla p = \mu \Delta \mathbf{v}, & \mathbf{x} \in \Omega^F, \\ \nabla \cdot \mathbf{v} = 0, & \mathbf{x} \in \Omega^F, \\ \mathbf{v}(x, -H, t) = 0, \end{cases} & \text{Solid: } & \begin{cases} \bar{\rho} \frac{\partial^2 \bar{u}_2}{\partial t^2} = \bar{\rho} \bar{c}_p^2 \Delta \bar{u}_2, & \mathbf{x} \in \Omega^S, \\ u_2(x, \bar{H}, t) = 0, \end{cases} \\
 \text{Interface: } & v_1 = 0, \quad v_2 = \frac{\partial \bar{u}_2}{\partial t}, \quad -p + 2\mu \frac{\partial v_2}{\partial y} = \bar{\rho} \bar{c}_p^2 \frac{\partial \bar{u}_2}{\partial y}, \quad \mathbf{x} \in \Gamma.
 \end{aligned}$$

Model Problem MP-VE. *Model problem MP-VE defines a viscous incompressible fluid and an elastic solid,*

$$\begin{aligned}
 \text{Fluid: } & \begin{cases} \rho \frac{\partial \mathbf{v}}{\partial t} + \nabla p = \mu \Delta \mathbf{v}, & \mathbf{x} \in \Omega^F, \\ \nabla \cdot \mathbf{v} = 0, & \mathbf{x} \in \Omega^F, \\ \mathbf{v}(x, -H, t) = 0, \end{cases} & \text{Solid: } & \begin{cases} \bar{\rho} \frac{\partial^2 \bar{\mathbf{u}}}{\partial t^2} = (\bar{\lambda} + \bar{\mu}) \nabla (\nabla \cdot \bar{\mathbf{u}}) + \bar{\mu} \Delta \bar{\mathbf{u}}, & \mathbf{x} \in \Omega^S, \\ \bar{\mathbf{u}}(x, \bar{H}, t) = 0, \end{cases} \\
 \text{Interface: } & \mathbf{v} = \frac{\partial \bar{\mathbf{u}}}{\partial t}, \quad \mu \left(\frac{\partial v_1}{\partial y} + \frac{\partial v_2}{\partial x} \right) = \bar{\mu} \left(\frac{\partial \bar{u}_1}{\partial y} + \frac{\partial \bar{u}_2}{\partial x} \right), \quad -p + 2\mu \frac{\partial v_2}{\partial y} = \bar{\lambda} \nabla \cdot \bar{\mathbf{u}} + 2\bar{\mu} \frac{\partial \bar{u}_2}{\partial y}, \quad \mathbf{x} \in \Gamma.
 \end{aligned}$$

5. An illustration of the AMP algorithm

As an illustration of the AMP algorithm, it is helpful to consider, as a representative FSI problem, a one-dimensional version of model problem MP-IA given in (32). While this one-dimensional problem is relatively simple, it does provide useful insight into the properties of the algorithm. To be consistent with the geometry of the two-dimensional problem, the one-dimensional problem varies in the y direction, with x fixed. Consider then an inviscid fluid in the domain $\Omega^F = \{y \in (-H, 0)\}$ adjacent to a solid in the domain $\Omega^S = \{y \in (0, \infty)\}$ with interface at $y = 0$ (and where $\bar{H} \rightarrow \infty$). For this one-dimensional problem, the velocity-pressure form of the equations in (14) and (15) for the fluid reduces to

$$\rho \frac{\partial v}{\partial t} + \frac{\partial p}{\partial y} = 0, \quad \frac{\partial^2 p}{\partial y^2} = 0, \quad y \in \Omega^F, \quad (33)$$

where $v = v_2$ and we assume the traction boundary condition $p(-H, t) = 0$. The equations in (18) and (19) for the solid become

$$\bar{\rho} \frac{\partial \bar{v}}{\partial t} = \frac{\partial \bar{\sigma}}{\partial y}, \quad \frac{\partial \bar{\sigma}}{\partial t} = \bar{\rho} \bar{c}_p \frac{\partial \bar{v}}{\partial y}, \quad y \in \Omega^S, \quad (34)$$

where $\bar{v} = \bar{v}_2$ and $\bar{\sigma} = \bar{\rho} \bar{c}_p^2 \partial_y \bar{u}_2$. The system of equations for the solid can be written in the characteristic form

$$\frac{d}{dt}(\bar{\sigma} \pm \bar{z}_p \bar{v}) = 0, \quad \text{along} \quad \frac{dy}{dt} = \mp \bar{c}_p,$$

and the definitions for the incoming and outgoing characteristics at the interface in (8) and (10), respectively, become

$$\mathcal{A}(\bar{\sigma}, \bar{v}) = \bar{\sigma} - \bar{z}_p \bar{v}, \quad \mathcal{B}(\bar{\sigma}, \bar{v}) = \bar{\sigma} + \bar{z}_p \bar{v}, \quad y = 0.$$

The standard interface matching conditions are

$$v(0, t) = \bar{v}(0, t), \quad \sigma(0, t) = \bar{\sigma}(0, t), \quad (35)$$

where $\sigma = -p$. The equivalent AMP interface conditions corresponding to (12) and (13) are

$$\sigma + \bar{z}_p v = \mathcal{B}(\bar{\sigma}, \bar{v}), \quad \mathcal{A}(\bar{\sigma}, \bar{v}) = \sigma - \bar{z}_p v, \quad y = 0, \quad (36)$$

where the first and second conditions in (36) are thought of as the interface conditions for the fluid and solid, respectively. The alternate AMP conditions corresponding (22) and (13), suitable when solving the pressure equation, are

$$\sigma + \bar{z}_p \Delta t \frac{\partial v}{\partial t} = \bar{\sigma} + \bar{z}_p \Delta t \frac{\partial \bar{v}}{\partial t}, \quad \mathcal{A}(\bar{\sigma}, \bar{v}) = \sigma - \bar{z}_p v, \quad y = 0. \quad (37)$$

By combining the first two conditions in (36) and (37), it can be shown that

$$\frac{\partial}{\partial t}(v - \bar{v}) = -\frac{1}{\Delta t}(v - \bar{v}), \quad y = 0,$$

and thus if $v(0, t) = \bar{v}(0, t)$ at $t = 0$, then the velocities on the interface are equal for all time. Also, if $v(0, t) - \bar{v}(0, t)$ is equal to some small nonzero value (from numerical error), then the difference in the velocity rapidly approaches zero. Thus, the alternate version of the interface conditions in (37) is essentially equivalent to those in (35).

Given the solution at time $t - \Delta t$, the AMP algorithm proceeds first by taking a time step of the solution in the solid domain to obtain predicted values, $\bar{\sigma}^{(p)}$ and $\bar{v}^{(p)}$, which then may be used to obtain outgoing characteristic data on the interface. Note that in one dimension, this data, if obtained using the method of characteristics, is completely determined from the solution in the solid domain at $t - \Delta t$, and is independent of the solution in the fluid domain.

We now advance the solution in the fluid domain using the outgoing interface data obtained from the solid domain, which is a key step in the AMP algorithm. First consider the pressure sub-problem,

$$\frac{\partial^2 \sigma}{\partial y^2} = 0, \quad y \in (-H, 0),$$

with boundary conditions

$$\sigma = 0, \quad y = -H, \quad \sigma + \frac{\bar{z}_p \Delta t}{\rho} \frac{\partial \sigma}{\partial y} = \bar{\sigma}^{(p)} + \bar{z}_p \Delta t \frac{\partial \bar{v}^{(p)}}{\partial t}, \quad y = 0.$$

The boundary condition at $y = 0$ is obtained from the outgoing condition in (37) and the momentum equation for the fluid in (33). The solution of the pressure sub-problem is

$$\sigma(y, t) = \sigma^I(t) \left(1 + \frac{y}{H}\right) \quad (38)$$

where

$$\sigma^I(t) = \frac{M_r}{1 + M_r} \left(\bar{\sigma}^{(p)}(0, t) + \bar{z}_p \Delta t \frac{\partial \bar{v}^{(p)}}{\partial t}(0, t) \right). \quad (39)$$

Observe that the traction at the interface, σ^I , is determined by the (known) outgoing characteristic data from the solid domain and involves the *added-mass* ratio M_r given by

$$M_r = \frac{\rho H}{\bar{z}_p \Delta t} = \frac{\rho H}{\bar{\rho} \bar{c}_p \Delta t} = \frac{z_f}{\bar{z}_p},$$

where $z_f = \rho H / \Delta t$ (or $z_f = \rho v_f$ with $v_f = H / \Delta t$) is a measure of the fluid impedance. The quantity M_r may be interpreted as the ratio of the mass of the entire fluid domain, ρH , to the mass of the solid displaced by its characteristic velocity over a time Δt , given by $\bar{\rho} \bar{c}_p \Delta t$. It may also be interpreted as a ratio of the fluid to solid impedances. If M_r is small, then added-mass effects are in some sense small, and if M_r is large, then added-mass effects are large. It may seem odd that M_r becomes large (i.e. added-mass effects become large) as $\Delta y = \bar{c}_p \Delta t$ becomes small (with $\rho H / \bar{\rho}$ fixed), but this is consistent with the analysis of the traditional partitioned (TP) scheme in Section 6.4.

In the context of the one-dimensional model problem, the velocity sub-problem is

$$\rho \frac{\partial v}{\partial t} = \frac{\partial \sigma}{\partial y}, \quad y \in (-H, 0),$$

with the boundary condition

$$\frac{\partial v}{\partial y} = 0, \quad y = 0. \quad (40)$$

Integrating the momentum equation and using the solution in (38) of the pressure sub-problem, we find

$$v(y, t) = v(y, t - \Delta t) + \frac{1}{\rho H} \int_{t-\Delta t}^t \sigma^I(\tau) d\tau. \quad (41)$$

The solution for velocity in (41) is spatially uniform so that the boundary condition in (40) is satisfied identically. Setting $y = 0$ in (41) and using (39), we obtain

$$v(0, t) = v(0, t - \Delta t) + \frac{M_r}{\rho H(1 + M_r)} \left[\int_{t-\Delta t}^t \bar{\sigma}^{(p)}(0, \tau) d\tau + \bar{z}_p \Delta t \left(\bar{v}^{(p)}(0, t) - \bar{v}^{(p)}(0, t - \Delta t) \right) \right].$$

Assuming the fluid and solid velocities on the interface are equal at $t - \Delta t$, and using a simple approximation of the integral gives

$$v(0, t) = \frac{M_r}{1 + M_r} v(0, t - \Delta t) + \frac{1}{1 + M_r} \left[\bar{v}^{(p)}(0, t) + \frac{1}{\bar{z}_p} \bar{\sigma}^{(p)}(0, t) \right]. \quad (42)$$

We observe that the velocity on the interface at time t given in (42) from the solution of the equations in the fluid domain is an added-mass-weighted average of the velocity at $t - \Delta t$ and a velocity determined by the outgoing characteristic data from the solution in the solid domain.

The interface velocity v^I may be taken as the velocity in (41) (or the approximation in (42)) determined by the solution in the fluid domain, or it may be taken as the velocity,

$$\bar{v}^{(p)}(0, t) + \frac{1}{\bar{z}_p} \left(\bar{\sigma}^{(p)}(0, t) - \sigma^I(t) \right),$$

determined by the outgoing characteristic condition at the interface (c.f. (28)). In fact, by eliminating $v(0, t - \Delta t)$ in (42) in terms of σ^I using the approximation $v(0, t) = v(0, t - \Delta t) + \sigma^I \Delta t / (\rho H)$ to (41), equation (42) can be written as an impedance-weighted average of these two values

$$v^I(t) = v(0, t) = \frac{z_f}{z_f + \bar{z}_p} v(0, t) + \frac{\bar{z}_p}{z_f + \bar{z}_p} \bar{v}^{(p)}(0, t) + \frac{1}{z_f + \bar{z}_p} \left(\bar{\sigma}^{(p)}(0, t) - \sigma^I(t) \right),$$

which is the one-dimensional version of the formula in (30). In this one-dimensional problem, the definition of v_f as $v_f = H/\Delta t$ naturally appears. Given the velocity and traction at the interface, v^I and σ^I , respectively, the solution for the solid can now be fully determined by solving the governing equations in (34) together with the boundary data

$$\bar{\sigma}(0, t) - \bar{z}_p \bar{v}(0, t) = \sigma^I(t) - \bar{z}_p v^I(t),$$

from the incoming characteristic.

The above description follows the AMP algorithm for a simple FSI problem in one dimension. The key step in the algorithm, as mentioned previously, is the incorporation of outgoing characteristic data from the solid domain into the fluid domain. The application of the AMP algorithm to this simple FSI problem also illustrates the contribution of the added-mass ratio M_r . In addition, it can be confirmed that for $\rho H \ll \bar{z}_p \Delta t$ ($M_r \ll 1$) the algorithm approaches the standard TP algorithm (defined previously in Algorithm 3) with the interface velocity being primarily transmitted from the solid, while the traction comes primarily from the fluid. On the other hand, for $\rho H \gg \bar{z}_p \Delta t$ ($M_r \gg 1$) the AMP algorithm approaches an *anti-traditional algorithm* with the roles of fluid and solid reversed in the application of the boundary conditions at the interface for each domain. Note that the AMP scheme always tends to the anti-traditional scheme for Δt sufficiently small; this is consistent with the analysis in Sections 6.4 and 6.5 which indicates that the anti-traditional scheme is stable when Δy and Δt become sufficiently small, while the TP algorithm is not.

6. Analysis of a two-dimensional acoustic solid and an inviscid incompressible fluid

In this section, we perform a stability analysis of the AMP algorithm applied to the two-dimensional FSI model problem MP-IA. In this problem, the fluid is taken as inviscid and the solid is treated as an acoustic solid that only supports motion in the vertical direction. The governing equations for the model are given by (32). We consider a semi-infinite solid domain ($\bar{H} = \infty$) and look for solutions in the solid that have finite L_2 -norm (which implies the solutions decay to zero as $y \rightarrow \infty$). The bottom boundary condition on the fluid at $y = -H$ is chosen as $\sigma = 0$ (i.e. $p = 0$).

6.1. Discretization

We discretize the fluid and solid variables in the x direction using a uniform grid with spacing $\Delta x = L/(N_x + 1)$. The grid points are given by $x_\ell = \ell \Delta x$, $\ell = 0, 1, \dots, N_x$. The choice of discrete approximations to the x derivatives in the equations plays little role in the analysis. Therefore, it is convenient to use a pseudo-spectral approximation by expanding each component q of the solution $(\mathbf{q}, \bar{\mathbf{q}})$ in a discrete Fourier series of the form

$$q_\ell(y, t) = \sum_{k=-N_x/2}^{N_x/2} e^{2\pi i k x_\ell / L} \hat{q}_k(y, t), \quad \ell = 0, 1, 2, \dots, N_x, \quad (43)$$

where $q_\ell(y, t) \approx q(x_\ell, y, t)$ and $\hat{q}_k(y, t)$ are Fourier coefficients, and where N_x is assumed to be even for convenience. Transforming the governing equations to Fourier space leads to the following equations for the Fourier coefficients of the solution variables:

$$\bar{\rho} \partial_t \bar{v} = ik_x \bar{\sigma}_{21} + \partial_y \bar{\sigma}_{22}, \quad y \in (0, \infty), \quad (44)$$

$$\partial_t \bar{\sigma}_{22} = \bar{\rho} \bar{c}_p^2 \partial_y \bar{v}, \quad y \in (0, \infty), \quad (45)$$

$$\partial_t \bar{\sigma}_{21} = ik_x \bar{\rho} \bar{c}_p^2 \bar{v}, \quad y \in (0, \infty), \quad (46)$$

$$\rho \partial_t v_1 = ik_x \sigma, \quad y \in (-H, 0), \quad (47)$$

$$\rho \partial_t v_2 = \partial_y \sigma, \quad y \in (-H, 0), \quad (48)$$

$$ik_x v_1 + \partial_y v_2 = 0, \quad y \in (-H, 0), \quad (49)$$

where $k_x = 2\pi k/L$ is a normalized wave number in the x direction and the equations hold for each $k = -N_x/2, -N_x/2 + 1, \dots, N_x/2$. The hats on the Fourier coefficients, along with the k subscripts, have been dropped for notational convenience. Note that the horizontal component of the fluid velocity, v_1 , is decoupled from the other equations and boundary conditions, and can be determined once v_2 is known. Equations (47)–(49) are used to obtain

$$\partial_y^2 \sigma - k_x^2 \sigma = 0, \quad y \in (-H, 0),$$

which is a Laplace equation for pressure (in Fourier space). The equations for the Fourier coefficients of the solid variables will be discretized using an upwind scheme. In preparation for this, it is convenient to define the characteristic variables

$$a = \bar{\sigma}_{22} - \bar{\rho} \bar{c}_p \bar{v}, \quad b = \bar{\sigma}_{22} + \bar{\rho} \bar{c}_p \bar{v}, \quad d = \bar{\sigma}_{21},$$

which, from (44)–(46), satisfy

$$\partial_t a + \bar{c}_p \partial_y a = ik_x \bar{c}_p d, \quad y \in (0, \infty), \quad (50)$$

$$\partial_t b - \bar{c}_p \partial_y b = -ik_x \bar{c}_p d, \quad y \in (0, \infty), \quad (51)$$

$$\partial_t d = \frac{ik_x \bar{c}_p}{2} (b - a), \quad y \in (0, \infty). \quad (52)$$

The solid variables are discretized in the y direction using a uniform grid with spacing Δy . The grid points for the solid domain are defined as $y_j = (j - \frac{1}{2})\Delta y$, $j = 0, 1, 2, \dots$. Following the analysis in [1, 10], the grid is staggered with respect to the interface at $y = 0$ and has a ghost point at $j = 0$; use of a non-staggered grid leads to similar results. Let Δt be the time step and let $t^n = n\Delta t$. The equations (50)–(52) are discretized using the first-order upwind scheme,

$$\frac{a_j^{n+1} - a_j^n}{\Delta t} + \bar{c}_p \frac{(a_j^n - a_{j-1}^n)}{\Delta y} = ik_x \bar{c}_p d_j^n, \quad (53)$$

$$\frac{b_j^{n+1} - b_j^n}{\Delta t} - \bar{c}_p \frac{(b_{j+1}^n - b_j^n)}{\Delta y} = -ik_x \bar{c}_p d_j^n, \quad (54)$$

$$\frac{d_j^{n+1} - d_j^n}{\Delta t} = \frac{ik_x \bar{c}_p}{2} (b_j^{n+1} - a_j^{n+1}), \quad (55)$$

where $a_j^n \approx a(y_j, t^n)$, $b_j^n \approx b(y_j, t^n)$ and $d_j^n \approx d(y_j, t^n)$. Since we have used a non-dissipative pseudo-spectral approximation, rather than a two-dimensional upwind scheme, the right-hand side terms in (55) are taken at time t^{n+1} in order to stabilize the approximation. A von Neumann stability analysis of equations (53) and (54) (for a periodic problem in y) shows that this time-stepping scheme is stable under reasonable conditions on the constants $\lambda_y = \bar{c}_p \Delta t / \Delta y$ and $\lambda_x = \bar{c}_p k_x \Delta t$. The fluid variables are kept continuous in y in order to simplify the presentation; a discrete version can be introduced but this makes only insignificant changes to the fundamental results. We are thus led to the following semi-discrete approximation for the solid and fluid equations,

$$a_j^{n+1} = a_j^n - \lambda_y (a_j^n - a_{j-1}^n) - i\lambda_x d_j^n, \quad j = 1, 2, 3, \dots, \quad (56)$$

$$b_j^{n+1} = b_j^n + \lambda_y (b_{j+1}^n - b_j^n) + i\lambda_x d_j^n, \quad j = 0, 1, 2, \dots, \quad (57)$$

$$d_j^{n+1} = d_j^n + \frac{i\lambda_x}{2} (b_j^{n+1} - a_j^{n+1}), \quad j = 0, 1, 2, \dots, \quad (58)$$

$$v^{n+1} = v^n + \frac{\Delta t}{\rho} \partial_y \sigma^{n+1}, \quad y \in (-H, 0), \quad (59)$$

$$0 = \partial_y^2 \sigma^{n+1} - k_x^2 \sigma^{n+1}, \quad y \in (-H, 0), \quad (60)$$

where $v^n(y) = v(y, t^n)$ and $\sigma^n(y) = \sigma(y, t^n)$. For reference, the discrete values for the (Fourier coefficients of the) velocity and components of stress in the solid are related to the characteristic variables by

$$\bar{v}_j^n = \frac{1}{2\bar{z}_p} (b_j^n - a_j^n), \quad \bar{\sigma}_{22,j}^n = \frac{1}{2} (b_j^n + a_j^n), \quad \bar{\sigma}_{21,j}^n = d_j^n.$$

The conditions at the top and bottom boundaries are

$$|a_j^n|^2 + |b_j^n|^2 + |d_j^n|^2 \rightarrow 0, \quad \text{as } j \rightarrow \infty, \quad (61)$$

$$\sigma^n(-H) = 0. \quad (62)$$

Initial conditions are required to define a_j^0 , b_j^0 and d_j^0 for $j = 0, 1, 2, 3, \dots$, as well as $v^0(y)$ for $y \in (-H, 0)$, but these conditions are of no significance in the subsequent stability analysis.

Approximations to the interface conditions are needed to complete the discrete formulation of the FSI model problem, and various choices are possible depending on the algorithm used. For the AMP algorithm, the pressure Robin condition (26) is imposed on the fluid; this is derived from the outgoing characteristic variables (12). In addition, the incoming characteristic variable (13) is used to specify a condition on the solid. The latter condition uses an interface velocity defined in (30) based on an impedance-weighted average. First-order accurate approximations of these conditions are

$$\sigma^{n+1}(0) + \frac{\bar{z}_p \Delta t}{\rho} \sigma_y^{n+1}(0) = \bar{\sigma}_{22,1}^{n+1} + \bar{z}_p (\bar{v}_1^{n+1} - v^{I,n}) = b_1^{n+1} - \bar{z}_p v^{I,n}, \quad (63)$$

$$a_0^{n+1} = \sigma^{I,n+1} - \bar{z}_p v^{I,n+1}, \quad (64)$$

where $\sigma^{I,n} \equiv \sigma^n(0)$ and $v^{I,n}$ are the interface traction and velocity, respectively. The latter is given by the impedance-weighted average

$$\begin{aligned} v^{I,n+1} &= \frac{z_f}{z_f + \bar{z}_p} v^{n+1}(0) + \frac{\bar{z}_p}{z_f + \bar{z}_p} \bar{v}_1^{n+1} + \frac{1}{z_f + \bar{z}_p} (\sigma_{22,1}^{n+1} - \sigma^{I,n+1}) \\ &= \gamma v^{n+1}(0) + \frac{1-\gamma}{\bar{z}_p} (b_1^{n+1} - \sigma^{I,n+1}), \end{aligned} \quad (65)$$

where

$$\gamma = \frac{z_f}{z_f + \bar{z}_p},$$

and where z_f is a measure of the fluid impedance as introduced in Section 3.

The traditional partitioned (TP) algorithm uses the velocity from the solid as a boundary condition for the fluid and the traction from the fluid as a boundary condition for the solid. First-order accurate approximations of these conditions are

$$v^{n+1}(0) = \bar{v}_1^{n+1}, \quad (66)$$

$$\bar{\sigma}_{22,0}^{n+1} = \sigma^{n+1}(0). \quad (67)$$

It is also instructive to consider an anti-traditional algorithm in which the roles of the fluid and solid are reversed in the application of the partitioned interface conditions. Approximations of these conditions are

$$\sigma^{n+1}(0) = \bar{\sigma}_{22,1}^{n+1}, \quad (68)$$

$$a_0^{n+1} = \sigma^{n+1}(0) - \bar{z}_p v^{n+1}(0). \quad (69)$$

The condition in (69) is equivalent to setting the velocity of solid at the interface equal to the velocity in the fluid since the stresses have already been equilibrated in (68).

6.2. Stability analysis

To analyze the stability of the approximation in (56)–(60), we look for solutions of the form

$$a_j^n = A^n \tilde{a}_j, \quad b_j^n = A^n \tilde{b}_j, \quad d_j^n = A^n \tilde{d}_j, \quad v^n(y) = A^n \tilde{v}(y), \quad \sigma^n(y) = A^n \tilde{\sigma}(y),$$

where $A \in \mathbb{C}$ is the amplification factor, $(\tilde{a}_j, \tilde{b}_j, \tilde{d}_j)$ are grid functions, and $(\tilde{v}(y), \tilde{\sigma}(y))$ are functions for $y \in [-H, 0]$. Substituting these forms into (56)–(60) results in the following system of equations

$$A\tilde{a}_j = \tilde{a}_j - \lambda_y(\tilde{a}_j - \tilde{a}_{j-1}) - i\lambda_x\tilde{d}_j, \quad j = 1, 2, 3, \dots, \quad (70)$$

$$A\tilde{b}_j = \tilde{b}_j + \lambda_y(\tilde{b}_{j+1} - \tilde{b}_j) + i\lambda_x\tilde{d}_j, \quad j = 0, 1, 2, \dots, \quad (71)$$

$$A\tilde{d}_j = \tilde{d}_j + \frac{i\lambda_x}{2}A(\tilde{b}_j - \tilde{a}_j), \quad j = 0, 1, 2, \dots, \quad (72)$$

$$A\tilde{v}(y) = \tilde{v}(y) + A\Delta t \tilde{\sigma}^I \frac{k_x \cosh(k_x(y+H))}{\rho \sinh(k_x H)}, \quad y \in [-H, 0], \quad (73)$$

$$\tilde{\sigma}(y) = \tilde{\sigma}^I \frac{\sinh(k_x(y+H))}{\sinh(k_x H)}, \quad y \in [-H, 0]. \quad (74)$$

To obtain (73) and (74), the ODE in (60) was integrated using the boundary conditions $\tilde{\sigma}(-H) = 0$ and $\tilde{\sigma}(0) = \tilde{\sigma}^I$, where the fluid stress at the interface, $\tilde{\sigma}^I$, is as yet unspecified. Note that the solution in the one-dimensional case, $k_x = 0$, is a special case that can be found by taking the limit $k_x \rightarrow 0$ in (73) and (74). Together with the interface conditions, equations (70)–(74) define a homogeneous set of difference equations. These equations have non-trivial solutions (i.e. eigenfunctions) only for particular values of A (i.e. eigenvalues). The scheme is said to be weakly stable, or stable in the sense of Godunov-Ryabenkii, for given values of the parameters Δt , Δy , k_x , H , etc., if there are no solutions (i.e. eigenfunctions) to this eigenvalue problem with $|A| > 1$. The *region of stability* of the scheme is the region in parameter space where there are no roots with $|A| > 1$. In order to delineate the stability region it is generally easier to look for regions where the scheme is *not* stable. Therefore, we assume that $|A| > 1$ and look for solutions to the eigenvalue problem.

Equations (70)–(72) are a system of constant-coefficient difference equations for the solid characteristic variables. After solving for \tilde{d}_j from (72) and substituting into (70) and (71), \tilde{a}_j and \tilde{b}_j are found to satisfy the recursion

$$\begin{bmatrix} \tilde{a}_j \\ \tilde{b}_j \end{bmatrix} = K \begin{bmatrix} \tilde{a}_{j-1} \\ \tilde{b}_{j-1} \end{bmatrix}, \quad K = \begin{bmatrix} (1 - \theta^2)/R & -\theta \\ \theta & R \end{bmatrix}, \quad (75)$$

where

$$R = r - \theta, \quad r = \frac{A - 1 + \lambda_y}{\lambda_y}, \quad \theta = -\frac{A\lambda_x^2}{2\lambda_y(A - 1)}. \quad (76)$$

The eigenvalues, ϕ_- and ϕ_+ , of the 2×2 matrix K in (75) are given by

$$\phi_- = B - \sqrt{B^2 - 1}, \quad \phi_+ = 1/\phi_-, \quad B = \frac{1}{2} \left(R + \frac{1 - \theta^2}{R} \right). \quad (77)$$

Note that the product of the eigenvalues is one. If both eigenvalues had magnitude equal to one, then there would be no solution of the recursion in (75) satisfying the boundary condition (61). Therefore, for a valid solution, there is one eigenvalue (either ϕ_- or ϕ_+), denoted by ϕ_s (for *small* ϕ), that has magnitude strictly less than one, i.e. $|\phi_s| < 1$. Let $\phi_b = 1/\phi_s$ (for *big* ϕ) be the other eigenvalue with $|\phi_b| > 1$. Note that when $\theta = 0$, $0 < \lambda_y \leq 1$, and $|A| > 1$, then $\phi_s = \phi_- = 1/r$ (but in general ϕ_s is not always equal to ϕ_-). Given that the eigenvalues are distinct, K can be diagonalized as

$$K = S^{-1}\Phi S, \quad \Phi = \begin{bmatrix} \phi_s & 0 \\ 0 & \phi_b \end{bmatrix}, \quad S = \begin{bmatrix} R - \phi_s & \theta \\ R - \phi_b & \theta \end{bmatrix}.$$

By setting

$$\begin{bmatrix} \alpha_j \\ \beta_j \end{bmatrix} = S \begin{bmatrix} \tilde{a}_j \\ \tilde{b}_j \end{bmatrix} = \begin{bmatrix} (R - \phi_s)\tilde{a}_j + \theta\tilde{b}_j \\ (R - \phi_b)\tilde{a}_j + \theta\tilde{b}_j \end{bmatrix}, \quad (78)$$

the general solution of the recursion in (75) is given by

$$\begin{aligned} \alpha_j &= \phi_s^j \alpha_0, \\ \beta_j &= \phi_b^j \beta_0. \end{aligned} \quad (79)$$

Since the solution must decay to zero as $j \rightarrow \infty$ and since $|\phi_b| > 1$, it follows that $\beta_0 = 0$ and thus $\beta_j = 0$ for all $j = 0, 1, 2, \dots$. Since $\beta_j = 0$, it follows from (78) that

$$\tilde{b}_j = Q\tilde{a}_j, \quad \alpha_j = (\phi_b - \phi_s)\tilde{a}_j, \quad Q = \frac{\phi_b - R}{\theta}, \quad (80)$$

and thus from (79),

$$\tilde{a}_j = \phi_s^j \tilde{a}_0.$$

Whence,

Proposition 1. *Solutions to the system in (70)–(74) with $|A| > 1$ satisfying the boundary conditions in (61) and (62) are given by*

$$\begin{aligned} \tilde{a}_j &= \phi_s^j \tilde{a}_0, & \tilde{b}_j &= Q\tilde{a}_j, & \tilde{d}_j &= \frac{i\lambda_x(Q-1)A}{2(A-1)}\tilde{a}_j, & j &= 0, 1, 2, \dots, \\ \tilde{\sigma}(y) &= \tilde{\sigma}^I \frac{\sinh(k_x(y+H))}{\sinh(k_xH)}, & \tilde{v}(y) &= \tilde{\sigma}^I \frac{A\Delta t}{A-1} \frac{k_x \cosh(k_x(y+H))}{\rho \sinh(k_xH)}, & y &\in [-H, 0], \end{aligned}$$

where \tilde{a}_0 and $\tilde{\sigma}^I$ are free constants.

The remaining constraints needed to complete the eigenvalue problem, which then determines the amplification factor A , are provided by two interface conditions. Choices for these interface conditions are discussed in the subsections below.

6.3. AMP interface conditions

Imposing the AMP interface conditions in (63) and (64) with the formula for the interface velocity in (65) gives

$$A\tilde{\sigma}^I = \eta \left(A\tilde{b}_1 - \bar{z}_p \tilde{v}^I \right), \quad (81)$$

$$\tilde{a}_0 = \tilde{\sigma}^I - \bar{z}_p \tilde{v}^I, \quad (82)$$

$$\tilde{v}^I = \gamma \tilde{v}(0) + \frac{1-\gamma}{\bar{z}_p} (\tilde{b}_1 - \tilde{\sigma}^I), \quad (83)$$

where

$$\eta \equiv \frac{1}{1 + \frac{\bar{z}_p k_x \Delta t}{\rho} \coth(k_x H)} = \frac{1}{1 + \frac{\bar{\rho} \lambda_x}{\rho} \coth(k_x H)}.$$

From (73) and (81) we also have

$$(A-1)\tilde{v}(0) = \frac{1-\eta}{\bar{z}} (A\tilde{b}_1 - \bar{z}\tilde{v}^I). \quad (84)$$

Using $\tilde{b}_1 = Q\phi_s\tilde{a}_0$ to eliminate \tilde{b}_1 in terms of \tilde{a}_0 and using (81) to eliminate $\tilde{\sigma}^I$, equations (82), (84) and (83) can be written in the form

$$\begin{bmatrix} A(1-\eta Q\phi_s) & 0 & A+\eta \\ (1-\eta)AQ\phi_s & 1-A & \eta-1 \\ -(1-\gamma)(1-\eta)Q\phi_s & -\gamma & 1-(1-\gamma)\eta A^{-1} \end{bmatrix} \begin{bmatrix} \tilde{a}_0 \\ \bar{z}\tilde{v}(0) \\ \bar{z}\tilde{v}^I \end{bmatrix} = 0. \quad (85)$$

The determinant of the matrix in (85) must be zero for non-trivial solutions to exist, and this leads to the following equation for A :

$$(A - (1 - \gamma)) (A - \eta - ((2\eta - 1)A - \eta)Q\phi_s) = 0.$$

Since $A - (1 - \gamma) \neq 0$ when $|A| > 1$ and $0 \leq \gamma \leq 2$, we have the following result.

Theorem 1. *The AMP interface approximation to the scheme (56)–(60) with boundary conditions (61) and (62), interface conditions (63) and (64), and interface velocity (65) is weakly stable if and only if $0 \leq \gamma \leq 2$ and there are no roots A with $|A| > 1$ to the equation*

$$f(A) \equiv A - \eta - \left((2\eta - 1)A - \eta \right) Q\phi_s = 0. \quad (86)$$

Note that $f(A)$ does not depend on γ , i.e. the weighting in the definition of the interface velocity, and thus the stability of the scheme is independent of γ provided $0 \leq \gamma \leq 2$. From a numerical conditioning point of view, however, we recommend the choice $\gamma = z_f / (z_f + \bar{z}_p)$ as used in (65).

Reduction to a polynomial equation for A . To examine the stability of the AMP algorithm we must consider all solutions of $f(A) = 0$. The function $f(A)$ in (86) involves square roots of A through the eigenvalues, ϕ_s and ϕ_b , of the matrix K in (75) and the definition of Q in (80). To ensure that all possible solutions are found, a polynomial $P(A)$ can be derived whose roots include all the roots of $f(A)$. To this end, note that from the definition for Q and $\phi_s\phi_b = 1$ it follows that

$$Q\phi_s = \frac{1 - R\phi_s}{\theta}.$$

Thus f is a linear function of ϕ_s since f only depends on the product $Q\phi_s$. Note also that $Q\phi_s$ is a rational function of A according to the definitions of R and θ in (76). Thus, $f(A) = 0$ can be written in the form

$$\phi_s = F(A),$$

where F is a rational function of A . Since ϕ_s is equal to one of the two eigenvalues, ϕ_{\pm} , defined in (77), it follows that

$$\pm\sqrt{B^2 - 1} = F(A) - B, \quad (87)$$

where the sign in front of the square root is chosen to be consistent with $|\phi_s| < 1$. Upon squaring both sides of (87), which introduces new roots, one obtains

$$P(A) = 0, \quad (88)$$

where $P(A)$ is a polynomial (as described below). We have thus shown the following:

Proposition 2. *Any solution of $f(A) = 0$ is also a root of the polynomial $P(A)$.*

All of the roots of $P(A)$ can be found numerically using well-developed algorithms (e.g. solving the eigenvalue problem for the companion matrix). In deriving $P(A)$, however, new roots have been introduced. Therefore, each root A^* of $P(A)$ must be checked to ensure that it is also solution of $f(A) = 0$.

Proposition 3. *A root, A^* , of $P(A)$ is also a root of $f(A)$, if ϕ_s in the definition of f satisfies*

$$\phi_s = \begin{cases} \phi_-(A^*) & \text{if } |\phi_-(A^*)| < 1, \\ \phi_+(A^*) & \text{otherwise,} \end{cases}$$

and if $f(A^*) = 0$.

The polynomial in (88) is (after removing uninteresting factors of $A - 1$) a polynomial of degree 5 given by

$$P_{\text{AMP}}(A) = \alpha_5 A^5 + \alpha_4 A^4 + \alpha_3 A^3 + \alpha_2 A^2 + \alpha_1 A + \alpha_0,$$

where the coefficients in the polynomial are

$$\begin{aligned} \alpha_0 &= -\eta^2 + 2\eta^2\lambda_y, \\ \alpha_1 &= -8\eta^2\lambda_y + 5\eta^2 - \lambda_x^2\eta^2, \\ \alpha_2 &= 10\eta^2\lambda_y - 9\eta^2 + 1 + 3\lambda_x^2\eta^2 + 4\eta\lambda_y - 2\eta - 2\lambda_y, \\ \alpha_3 &= -2\lambda_y\lambda_x^2 - 2\eta\lambda_x^2 + 4\lambda_y + \lambda_x^2 + 4\eta\lambda_y\lambda_x^2 + 7\eta^2 - 3 + 6\eta - 4\eta^2\lambda_y - 8\eta\lambda_y - 2\eta^2\lambda_y\lambda_x^2 - 2\lambda_x^2\eta^2, \\ \alpha_4 &= 3 - 2\lambda_y - 2\eta^2 - \lambda_x^2 + 4\eta\lambda_y - 6\eta + 2\eta\lambda_x^2, \\ \alpha_5 &= -1 + 2\eta. \end{aligned}$$

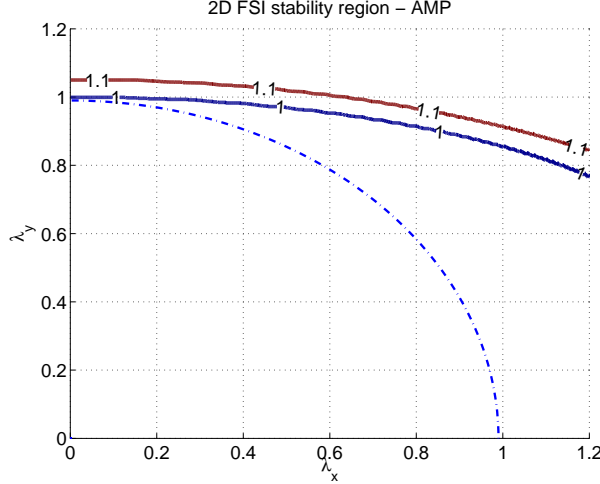


Figure 2: Stability region for the two-dimensional model problem using the AMP algorithm. The curve marked 1 is the curve for which $\max_{0 \leq \eta \leq 1} |A| = 1$. The curve for which $\max_{0 \leq \eta \leq 1} |A| = 1.1$ is shown for reference. The dashed curve shows the curve $\lambda_x^2 + \lambda_y^2 = (.99)^2$.

It turns out that $P_{\text{AMP}}(A)$ is the same polynomial generated by the Maple symbolic algebra program when asked to solve $f(A) = 0$.

To determine if there are any roots of $P_{\text{AMP}}(A)$ with $|A| > 1$, we evaluate the roots numerically for an array of parameter values in the region $0 < \lambda_x < 1.2$, $0 < \lambda_y < 1.2$ and $0 \leq \eta \leq 1$ with N_A equally spaced points in each parameter direction. The stability region of the scheme is the region in the space of $(\lambda_x, \lambda_y, \eta)$ where the magnitude of the largest valid root satisfies $|A| \leq 1$. This region is computed on a grid with $N_A = 800$ points for each parameter. In Figure 2, we plot the curve in the (λ_x, λ_y) plane for which $\max_{0 \leq \eta \leq 1} |A| = 1$. (The curve for which $\max_{0 \leq \eta \leq 1} |A| = 1.1$ is also plotted for reference.) Observe that the region of stability contains the region $0 \leq \eta \leq 1$ and $\lambda_x^2 + \lambda_y^2 \leq \kappa^2$ (for $\lambda_x \geq 0$ and $\lambda_y \geq 0$) where the maximum value for κ appears to be $\kappa = 1$. Further evidence for $\kappa = 1$ being the upper bound is provided by the restriction of the analysis to one dimension given below. The curve $\lambda_x^2 + \lambda_y^2 = (.99)^2$ is shown in the figure as an example. Since $\lambda_x = \bar{c}_p k_x \Delta t$ and $\lambda_y = \bar{c}_p \Delta t / \Delta y$, the condition $\lambda_x^2 + \lambda_y^2 \leq 1$ implies the following result.

Theorem 2. *By numerical evaluation of the stability polynomial, $P_{\text{AMP}}(A)$, we have found that the AMP algorithm is weakly stable (i.e. there are no valid roots of $P_{\text{AMP}}(A)$ with $|A| > 1$) provided $\lambda_x^2 + \lambda_y^2 \leq 1$, i.e.*

$$\Delta t \leq \frac{1}{\bar{c}_p} \left[\frac{1}{\Delta y^2} + k_x^2 \right]^{-1/2}.$$

This is a sufficient but not a necessary condition.

Note that the time step Δt satisfies a typical CFL constraint arising from the fastest wave speed in the solid. In the incompressible limit when $\bar{c}_p \rightarrow \infty$, the maximum stable Δt would go to zero, as it would for the solid in isolation. For incompressible solids, alternative formulations should be considered. Developing AMP algorithms for incompressible solids is a subject for future work.

Restriction to one space dimension. The stability of the one-dimensional version of the AMP algorithm may be examined by considering the special case of the two-dimensional algorithm with $\lambda_x = 0$ and $Q = 0$. In this case there are two solutions of $f(A) = 0$ given by

$$A = 1 - 2\lambda_y \quad \text{or} \quad A = \eta.$$

We are interested in whether there are solutions with $|A| > 1$. Since $0 \leq \eta \leq 1$ we have the result.

Theorem 3. *The one-dimensional AMP algorithm is weakly stable provided $0 \leq \gamma \leq 2$ and $0 \leq \lambda_y \leq 1$, i.e.*

$$\Delta t \leq \frac{\Delta y}{\bar{c}_p}.$$

For comparison, we now discuss briefly the corresponding stability results for the scheme given by (56)–(60) with boundary conditions (61) and (62), and with interface conditions given by either the traditional (TP) algorithm or the anti-traditional algorithm.

6.4. TP interface conditions

The interface conditions for the TP algorithm are given by (66) and (67). Following the previous analysis, A is found to satisfy

$$f_{\text{TP}}(A) \equiv A(Q+1) - \frac{\eta-1}{\eta}(A-1)(Q-1)\phi_s = 0. \quad (89)$$

Restriction to one space dimension. In one dimension, the condition in (89) reduces to the polynomial equation

$$P_{\text{TP}}(A) = A^2 + (\mathcal{M} + \lambda_y - 1)A - \mathcal{M} = 0, \quad \text{where } \mathcal{M} = \frac{\rho H}{\bar{\rho} \Delta y}.$$

(Here, all of the roots of this quadratic are valid since no spurious roots were introduced in deriving the equation.) The product of the roots is $-\mathcal{M}$ and thus a necessary condition for stability is that $|\mathcal{M}| \leq 1$. Thus the mass of the solid in a thin strip one grid cell wide, $\bar{\rho} \Delta y L$, must be larger than the mass of the entire fluid domain $\rho H L$. Using the theory of von Neumann polynomials [46, 47] one can show the following necessary and sufficient condition.

Theorem 4. *The one-dimensional TP algorithm is weakly stable if and only if*

$$\Delta t \leq \frac{2}{\bar{c}_p} \left(\Delta y - \frac{\rho H}{\bar{\rho}} \right).$$

This is a curious result. For a given *large* value of Δy the one-dimensional scheme may be stable, but it will eventually become unstable as the mesh is refined and Δy becomes less than $(\rho H)/\bar{\rho}$. The one-dimensional TP algorithm is thus formally *unconditionally unstable*. The numerical results in Section 8.2 show that this behaviour also holds for the second-order accurate discretization of the two-dimensional model problem MP-VE.

6.5. Anti-traditional interface conditions

The interface conditions for the anti-traditional algorithm are given by (68) and (69). The analysis for this choice leads to the constraint

$$f_{\text{AT}}(A) = 1 - A + \frac{1}{2} \left(\frac{2\eta-1}{\eta} A - 1 \right) (Q+1)\phi_s = 0. \quad (90)$$

Restriction to one space dimension. In one dimension, (90) reduces to the polynomial constraint

$$P_{\text{AT}}(A) = A^2 + \left(\frac{\lambda_y}{2} \left(1 + \frac{\lambda_y}{\mathcal{M}} \right) - 2 \right) A + 1 - \frac{\lambda_y}{2} = 0.$$

An analysis of the roots of $P_{\text{AT}}(A)$ leads us to the following result:

Theorem 5. *The one-dimensional anti-traditional algorithm is weakly stable if and only if $\lambda_y \leq 4$ and*

$$\Delta t \leq \frac{\Delta y}{\bar{c}_p} \left(\sqrt{\mathcal{M}^2 + 8\mathcal{M}} - \mathcal{M} \right). \quad (91)$$

We observe that the one-dimensional anti-traditional scheme is (weakly) stable for any value of the added-mass ratio $\mathcal{M} = (\rho H)/(\bar{\rho} \Delta y)$ provided that Δt is taken sufficiently small. The anti-traditional scheme is thus a stable alternative to the AMP scheme. However, in the *heavy solid* regime when \mathcal{M} is small, the anti-traditional requires a smaller Δt than the AMP scheme, scaling like $\sqrt{8\mathcal{M}}$ for $\mathcal{M} \ll 1$, as can be seen from (91).

7. The AMP FSI time-stepping algorithm

We now describe our implementation of the AMP algorithm, which is then used to obtain the numerical results presented in Section 8 for the three model problems defined in Section 4. The AMP algorithm was introduced in predictor form in Section 3. It is defined here in a more general form, as a predictor-corrector time-stepping scheme, in terms of various procedures which we outline below; additional details of the procedures are given in Appendix B. As mentioned earlier, the velocity-pressure form of the fluid equations are solved using a fractional-step scheme following [6, 7]. The viscous term, $\mu\Delta\mathbf{v}$, in the fluid momentum equation is advanced in time explicitly in the present implementation, but this term could also be treated implicitly with minor modifications. The fractional-step scheme for the fluid also uses a predictor-corrector scheme, consisting of a second-order accurate Adams-Bashforth predictor followed by a second-order accurate Adams-Moulton corrector (trapezoidal rule). Other time-stepping schemes for the fluid could also be used. We note that the AMP algorithm is stable even with no corrector step provided the predictor step in the fluid is stable in isolation. (The use of the Adams-Bashforth predictor for the fluid by itself requires sufficient physical or numerical dissipation for stability.) The solid is advanced explicitly as well using a second-order accurate upwind scheme for the solid equations written as a first-order system (17)–(19), following the approach in [8].

Let the grid functions $p_{\mathbf{i}}^{n-1} \approx p(\mathbf{x}_{\mathbf{i}}, t^{n-1})$ and $\mathbf{v}_{\mathbf{i}}^{n-1} \approx \mathbf{v}(\mathbf{x}_{\mathbf{i}}, t^{n-1})$ denote the discrete approximations to the fluid pressure and velocity, respectively, at grid points $\mathbf{x}_{\mathbf{i}}$ and at time t^{n-1} . Let $\bar{\mathbf{q}}_{\mathbf{i}}^{n-1} = (\bar{\mathbf{u}}_{\mathbf{i}}^{n-1}, \bar{\mathbf{v}}_{\mathbf{i}}^{n-1}, \bar{\boldsymbol{\sigma}}_{\mathbf{i}}^{n-1})^T$ denote a vector of grid functions for the solid displacement, velocity and stress, respectively. At the start of the time step, the discrete solution values at time t^{n-1} are assumed to be known at all grid points, including boundary and ghost points.

Begin predictor.

Stage 1: Advance the solid one time step to give a vector of predicted values $\bar{\mathbf{q}}_{\mathbf{i}}^{(p)} = (\bar{\mathbf{u}}_{\mathbf{i}}^{(p)}, \bar{\mathbf{v}}_{\mathbf{i}}^{(p)}, \bar{\boldsymbol{\sigma}}_{\mathbf{i}}^{(p)})^T$. Assign values at interior, boundary and interface points, including values for $\bar{\boldsymbol{\sigma}}_{\mathbf{i}}^{(p)} \mathbf{n}_{\mathbf{i}}$ on the interface. No boundary conditions are applied at this stage.

$$\bar{\mathbf{q}}_{\mathbf{i}}^{(p)} = \text{advanceSolid}(\bar{\mathbf{q}}_{\mathbf{i}}^{n-1})$$

Stage 2(a): Advance the fluid velocity one time step to give predicted values $\mathbf{v}_{\mathbf{i}}^{(p)}$. Assign values at interior, boundary and interface points.

$$\mathbf{v}_{\mathbf{i}}^{(p)} = \text{advanceFluid}(\mathbf{v}_{\mathbf{i}}^{n-1}, p_{\mathbf{i}}^{n-1}, \mathbf{v}_{\mathbf{i}}^{n-2}, p_{\mathbf{i}}^{n-2})$$

Stage 2(b): Compute extrapolated values for the fluid pressure and compute the projected interface velocity excluding traction terms in the formula for the interface velocity since these terms are not known at this stage. Assign boundary conditions on the fluid velocity using the AMP Robin condition (25) for the velocity.

$$\begin{aligned} p_{\mathbf{i}}^{(e)} &= \text{extrapolateInTime}(p_{\mathbf{i}}^{n-1}, p_{\mathbf{i}}^{n-2}, p_{\mathbf{i}}^{n-3}) \\ \mathbf{v}_{\mathbf{i}}^I &= \text{projectInterfaceVelocity}(\mathbf{v}_{\mathbf{i}}^{(p)}, p_{\mathbf{i}}^{(e)}, \bar{\mathbf{v}}_{\mathbf{i}}^{(p)}, \bar{\boldsymbol{\sigma}}_{\mathbf{i}}^{(p)} \mathbf{n}_{\mathbf{i}}, \beta = 0) \\ (\mathbf{v}_{\mathbf{i}}^I, (\boldsymbol{\sigma} \mathbf{n})_{\mathbf{i}}^I) &= \text{assignFluidVelocityBoundaryConditions}(\mathbf{v}_{\mathbf{i}}^{(p)}, p_{\mathbf{i}}^{(e)}, \mathbf{v}_{\mathbf{i}}^I, \bar{\mathbf{v}}_{\mathbf{i}}^{(p)}, \bar{\boldsymbol{\sigma}}_{\mathbf{i}}^{(p)} \mathbf{n}_{\mathbf{i}}) \end{aligned}$$

Here $p_{\mathbf{i}}^{(e)}$, needed in the boundary conditions, is a second-order accurate approximation for the fluid pressure on the interface at time t^n obtained by extrapolation in time using past values $p_{\mathbf{i}}^m$, $m = n-1, n-2, n-3$. The parameter β in the procedure that computes the interface velocity is set to zero which specifies that the traction terms are not used.

Stage 3(a): Compute the solid acceleration, $\dot{\bar{\mathbf{v}}}_{\mathbf{i}}^{(p)}$, and solve for the fluid pressure using the AMP Robin pressure boundary condition (26). Assign values at interior, boundary and interface points, including ghost points.

$$\begin{aligned} \dot{\bar{\mathbf{v}}}_{\mathbf{i}}^{(p)} &= \text{computeSolidAcceleration}(\bar{\mathbf{v}}_{\mathbf{i}}^{(p)}, \bar{\mathbf{v}}_{\mathbf{i}}^n) \\ p_{\mathbf{i}}^{(p)} &= \text{solveFluidPressureEquation}(\mathbf{v}_{\mathbf{i}}^{(p)}, \bar{\mathbf{v}}_{\mathbf{i}}^{(p)}, \bar{\boldsymbol{\sigma}}_{\mathbf{i}}^{(p)} \mathbf{n}_{\mathbf{i}}, \dot{\bar{\mathbf{v}}}_{\mathbf{i}}^{(p)}) \end{aligned}$$

Here $\dot{\mathbf{v}}_i^{(p)}$, used for the pressure boundary condition, is a second-order accurate approximation to the solid acceleration on the interface at t^n .

Stage 3(b) : Given $p_i^{(p)}$, recompute the interface velocity and traction, and then assign solid boundary conditions.

$$\begin{aligned} \mathbf{v}_i^I &= \text{projectInterfaceVelocity}(\mathbf{v}_i^{(p)}, p_i^{(p)}, \bar{\mathbf{v}}_i^{(p)}, \bar{\boldsymbol{\sigma}}_i^{(p)} \mathbf{n}_i, \beta = 1) \\ (\mathbf{v}_i^I, (\boldsymbol{\sigma} \mathbf{n})_i^I) &= \text{assignFluidVelocityBoundaryConditions}(\mathbf{v}_i^{(p)}, p_i^{(p)}, \mathbf{v}_i^I, \bar{\mathbf{v}}_i^{(p)}, \bar{\boldsymbol{\sigma}}_i^{(p)} \mathbf{n}_i) \\ (\bar{\mathbf{v}}_i^{(p)}, \bar{\boldsymbol{\sigma}}_i^{(p)} \mathbf{n}_i) &= \text{assignSolidBoundaryConditions}(\bar{\mathbf{v}}_i^{(p)}, \bar{\boldsymbol{\sigma}}_i^{(p)}, \mathbf{v}_i^I, (\boldsymbol{\sigma} \mathbf{n})_i^I) \end{aligned}$$

The parameter β in the procedure that computes the interface velocity is now set to one which specifies that the traction terms are used.

End predictor.

If the predictor step is used alone (without the corrector step), then discrete values for p_i^n and \mathbf{v}_i^n in the fluid, and for $\bar{\mathbf{q}}_i^n = (\bar{\mathbf{u}}_i^n, \bar{\mathbf{v}}_i^n, \bar{\boldsymbol{\sigma}}_i^n)^T$ in the solid, are taken from the corresponding predicted values and the time step to t^n is complete. If, on the other hand, a corrector step is used, then stages 4–7 are included in the algorithm as given below.

Begin corrector: (optional)

Stage 4 : Correct the solid to obtain $\bar{\mathbf{q}}_i^n = (\bar{\mathbf{u}}_i^n, \bar{\mathbf{v}}_i^n, \bar{\boldsymbol{\sigma}}_i^n)^T$. Assign values at interior, boundary and interface points.

$$\bar{\mathbf{q}}_i^n = \text{correctSolid}(\bar{\mathbf{q}}_i^{(p)}, \bar{\mathbf{q}}_i^{n-1})$$

Stage 5(a) : Correct the fluid velocity to obtain \mathbf{v}_i^n . Assign interior, boundary and interface points.

$$\mathbf{v}_i^n = \text{correctFluid}(\mathbf{v}_i^{(p)}, p_i^{(p)}, \mathbf{v}_i^{n-1}, p_i^{n-1})$$

Stage 5(b) : Assign fluid boundary conditions (assigns boundary/interface and ghost points).

$$\begin{aligned} \mathbf{v}_i^I &= \text{projectInterfaceVelocity}(\mathbf{v}_i^n, p_i^n, \bar{\mathbf{v}}_i^n, \bar{\boldsymbol{\sigma}}_i^n \mathbf{n}_i, \beta = 1) \\ (\mathbf{v}_i^I, (\boldsymbol{\sigma} \mathbf{n})_i^I) &= \text{assignFluidVelocityBoundaryConditions}(\mathbf{v}_i^n, p_i^n, \mathbf{v}_i^I, \bar{\mathbf{v}}_i^n, \bar{\boldsymbol{\sigma}}_i^n \mathbf{n}_i) \end{aligned}$$

Stage 6: Correct the fluid pressure. Assign values at interior, boundary and interface points, including ghost points.

$$\begin{aligned} \dot{\mathbf{v}}_i &= \text{computeSolidAcceleration}(\bar{\mathbf{v}}_i^n, \bar{\mathbf{v}}_i^{n-1}) \\ p_i^n &= \text{solveFluidPressureEquation}(\mathbf{v}_i^n, \bar{\mathbf{v}}_i^n, \bar{\boldsymbol{\sigma}}_i^n \mathbf{n}_i, \dot{\mathbf{v}}_i) \end{aligned}$$

Stage 7 : Re-compute interface velocity using corrected pressure, and re-assign the fluid boundary conditions. Assign solid boundary conditions using latest values for \mathbf{v}_i^I and $\boldsymbol{\sigma}_i^I$.

$$\begin{aligned} \mathbf{v}_i^I &= \text{projectInterfaceVelocity}(\mathbf{v}_i^n, p_i^n, \bar{\mathbf{v}}_i^n, \bar{\boldsymbol{\sigma}}_i^n \mathbf{n}_i, \beta = 1) \\ (\mathbf{v}_i^I, (\boldsymbol{\sigma} \mathbf{n})_i^I) &= \text{assignFluidVelocityBoundaryConditions}(\mathbf{v}_i^n, p_i^n, \mathbf{v}_i^I, \bar{\mathbf{v}}_i^n, \bar{\boldsymbol{\sigma}}_i^n \mathbf{n}_i) \\ (\bar{\mathbf{v}}_i^n, \bar{\boldsymbol{\sigma}}_i^n \mathbf{n}_i) &= \text{assignSolidBoundaryConditions}(\bar{\mathbf{v}}_i^n, \bar{\boldsymbol{\sigma}}_i^n, \mathbf{v}_i^I, (\boldsymbol{\sigma} \mathbf{n})_i^I) \end{aligned}$$

end corrector

The corrector step described above may be repeated, replacing the predicted states with the latest solution values. This may permit a somewhat larger time step but also involves an additional cost. For all calculations presented in the next section we use the predictor step with just one corrector step.

8. Numerical results

In this section, we present numerical results based on the model problems in Section 4 to verify the accuracy and stability of the AMP algorithm. All of the model problems consist of a rectangular fluid domain, $\Omega^F = (0, L) \times (-H, 0)$, and a rectangular solid domain, $\Omega^S = (0, L) \times (0, \bar{H})$, connected by an interface, $\Gamma = \{(x, y) | x \in (0, L), y = 0\}$. We use a Cartesian grid for the fluid domain with $N_j + 1$ grid points in each direction so that the grid spacings are $\Delta x_j = L/N_j$ and $\Delta y_j = H/N_j$. (The subscript j is used later to indicate the resolution of the grid.) The grid for the solid domain is also a Cartesian grid and uses the same grid spacing as the fluid grid. For all calculations we take

$$\rho = 1, \quad L = 1, \quad H = 1, \quad \bar{\rho} = \bar{\lambda} = \bar{\mu} = \rho \delta, \quad \bar{H} = 1/2,$$

where the *density ratio* $\delta = \bar{\rho}/\rho$ is a parameter that is chosen later to consider the cases of light, medium and heavy solids. The value for the fluid viscosity, μ , is chosen based on the different model problems. The value for the fluid impedance, z_f , used in the velocity projection (30) and (31), is taken as $z_f = \rho \Delta y_j / \Delta t_j$ following the discussion in Section 5, however the results are insensitive to this choice. The solid equations are evolved using a second-order accurate upwind scheme with all solid variables being co-located at the nodes, see [8] for more details. The fluid equations are discretized using standard second-order accurate, central finite difference approximations with the velocity and pressure variables being co-located on the nodes. For more details, see [6, 7]. Note that in the linearized approximation, the fluid domain remains fixed in time and thus there is no moving grid.

We begin by considering solutions of the model problems constructed using the method of analytic solutions. These are compared with numerical approximations computed using the AMP algorithm for different values of density ratio. We then consider numerical solutions of the model problems for cases where exact traveling wave solutions are known.

MP-VA, trigonometric solution, viscous fluid, $\mu = .05$, heavy acoustic solid, $\delta = 10^3$										
h_j	$E_j^{(p)}$	r	$E_j^{(v)}$	r	$E_j^{(\bar{u})}$	r	$E_j^{(\bar{v})}$	r	$E_j^{(\bar{\sigma})}$	r
1/20	1.6e-2		4.0e-2		7.6e-3		4.0e-2		1.1e2	
1/40	2.1e-2	0.7	8.0e-3	5.0	1.5e-3	5.2	8.1e-3	4.9	1.6e1	7.0
1/80	7.6e-3	2.7	1.9e-3	4.2	3.4e-4	4.4	2.2e-3	3.6	1.6e0	9.5
1/160	1.5e-3	5.1	4.6e-4	4.2	8.0e-5	4.2	5.8e-4	3.8	1.9e-1	8.5
1/320	2.7e-4	5.6	1.1e-4	4.1	1.9e-5	4.1	1.5e-4	3.9	5.3e-2	3.7
rate	1.55		2.11		2.14		2.00		2.83	

MP-VA, trigonometric solution, viscous fluid, $\mu = .05$, medium acoustic solid, $\delta = 1$										
h_j	$E_j^{(p)}$	r	$E_j^{(v)}$	r	$E_j^{(\bar{u})}$	r	$E_j^{(\bar{v})}$	r	$E_j^{(\bar{\sigma})}$	r
1/20	2.1e-2		2.2e-2		5.4e-3		2.5e-2		4.6e-2	
1/40	6.1e-3	3.4	3.9e-3	5.6	1.3e-3	4.0	6.7e-3	3.8	9.3e-3	5.0
1/80	1.8e-3	3.3	7.4e-4	5.2	3.2e-4	4.2	1.9e-3	3.6	2.2e-3	4.1
1/160	4.6e-4	4.0	1.5e-4	4.8	7.8e-5	4.1	5.1e-4	3.7	5.3e-4	4.3
rate	1.82		2.38		2.04		1.87		2.14	

MP-VA, trigonometric solution, viscous fluid, $\mu = .05$, light acoustic solid, $\delta = 10^{-1}$										
h_j	$E_j^{(p)}$	r	$E_j^{(v)}$	r	$E_j^{(\bar{u})}$	r	$E_j^{(\bar{v})}$	r	$E_j^{(\bar{\sigma})}$	r
1/20	7.0e-3		8.0e-3		3.0e-3		3.4e-2		8.4e-3	
1/40	1.3e-3	5.4	1.2e-3	6.5	8.6e-4	3.5	7.9e-3	4.2	1.9e-3	4.5
1/80	2.7e-4	4.8	2.0e-4	6.2	2.3e-4	3.8	2.1e-3	3.7	3.8e-4	4.8
1/160	7.6e-5	3.6	3.7e-5	5.4	6.0e-5	3.8	5.6e-4	3.8	7.7e-5	5.0
rate	2.18		2.59		1.88		1.96		2.26	

Figure 3: Trigonometric exact solution for a viscous incompressible fluid and acoustic solid (model problem MP-VA). Maximum errors and estimated convergence rates at $t = 0.3$ computed using the AMP algorithm for a heavy solid, $\delta = 10^3$, medium solid, $\delta = 1$ and light solid, $\delta = 10^{-1}$.

8.1. The method of analytic solutions

The method of analytic solutions is a useful technique for constructing exact solutions of initial-boundary-value problems for partial differential equations for the purpose of checking the behavior and accuracy of the numerical implementation of a problem. This method, also known as the *method of manufactured solutions* [48] or *twilight-zone forcing* [49], adds forcing functions to the governing equations, boundary conditions and interface conditions. These forcing functions are specified so that a chosen function, $\tilde{\mathbf{q}}(\mathbf{x}, t)$, becomes the exact solution of the forced equations, and thus the error in the discrete solution can be computed exactly.

The method of analytic solutions is applied to the FSI problems using trigonometric functions. The exact solutions for the components of displacement, velocity and stress in the solid are taken to be

$$\begin{aligned} \tilde{u}_1 &= .25 c_1 \tilde{c}_2 c_t, & \tilde{u}_2 &= .5 c_1 \tilde{c}_2 c_t, & \tilde{v}_1 &= \dot{u}_1, & \tilde{v}_2 &= \dot{u}_2, \\ \tilde{\sigma}_{11} &= -.5 c_1 c_2 c_t, & \tilde{\sigma}_{12} &= .4 s_1 c_2 c_t, & \tilde{\sigma}_{21} &= .4 s_1 c_2 c_t, & \tilde{\sigma}_{22} &= .6 c_1 s_2 c_t, \end{aligned} \quad (92)$$

where $(c_1, s_1) = (\cos(2\pi x), \sin(2\pi x))$, $(c_2, s_2) = (\cos(2\pi y), \sin(2\pi y))$, $\tilde{c}_2 = \cos(2\pi(y + 0.375))$ and $c_t = \cos(2\pi t)$. The exact solutions for the pressure and the components of velocity in the fluid are

$$\tilde{p} = c_1 s_2 c_t, \quad \tilde{v}_1 = .5 c_1 c_2 c_t, \quad \tilde{v}_2 = .5 s_1 s_2 c_t. \quad (93)$$

These trigonometric functions are substituted into the differential equations governing each domain, and into the boundary and interface conditions, to define forcing functions to the equations so that the functions given above become exact solutions of the initial-boundary-value problem.

Numerical solutions of the (forced) model problems are computed using the AMP algorithm. The initial conditions for the numerical calculations are taken from the exact solutions evaluated at $t = 0$. For each case, maximum-norm errors, $E_j^{(q)}$, for solution component q , are computed on grids of increasing resolution using grid spacings $\Delta x_j = \Delta y_j = h_j = 1/(20j)$, $j = 1, 2, \dots$. The convergence rate, ζ_q , is estimated by a least squares fit to the logarithm of the error equation, $E_j^{(q)} = C_q h_j^{\zeta_q}$, where C_q is approximately constant for small grid spacings. For vector variables, such as \mathbf{v} or $\tilde{\boldsymbol{\sigma}}$, the error denotes the maximum over all components of the vector or tensor.

The tables in Figure 3 give the maximum errors and estimated convergence rates for the results of the AMP algorithm applied to the FSI problem of a viscous incompressible fluid and acoustic solid that only supports vertical motion (model problem MP-VA). Similar results are obtained for the other model problems. Results are presented for the density ratios $\delta = 10^3$, 1 and 10^{-1} , referred to as *heavy*, *medium* and *light* solids. The fluid viscosity is taken as $\mu = 0.05$ for each case. The values in the columns labeled “r” give the ratio of the error on the current grid to that on the previous coarser grid; a ratio of 4 is expected for a second-order accurate method. The values in the tables show that the scheme is stable and close to second-order accurate in the maximum-norm. For the heavy solid, $\delta = 10^3$, the stresses in the solid are very large, $\mathcal{O}(\rho \bar{c}_p^2)$, compared to the fluid stress, and this affects the convergence rates on coarser grids. Note that the errors given in the table (and subsequent tables below) are absolute errors. Thus, for the case of a heavy solid, the errors in the solid stress appear to be large even though the corresponding relative errors are small.

8.2. Traveling wave exact solutions

We now consider the three FSI model problems for cases when the exact solutions are traveling waves. The traveling waves have the form $q(x, y, t) = \hat{q}(y)e^{i(kx - \omega t)}$, where q represents any component of the variables belonging to the fluid or solid domains. The solutions are periodic in x with wave number $k \in \mathbb{R}$ and have frequency $\omega \in \mathbb{C}$ in time. For inviscid fluids (as in the MP-IA model problem), $\text{Im}(\omega) = 0$ so that the traveling wave is also periodic in time. For viscous fluids (as in the model problems MP-VA and MP-VE), $\text{Im}(\omega) < 0$ so that the amplitude of the traveling wave decays over time. For the results shown here, we take $k = 2\pi$ and a value for ω obtained from solving an appropriate dispersion relation (see Appendix A) such that the wave travels from left to right (i.e. $\text{Re}(\omega) > 0$). In all cases, periodic boundary conditions are used in the x direction. The amplitude parameter in the definition of the traveling wave solutions is chosen as $\bar{u}_{\max} = 1/10$, which defines the maximum amplitude of the displacement on the interface. The initial conditions for the numerical solutions are taken from the exact traveling wave solution evaluated at $t = 0$.

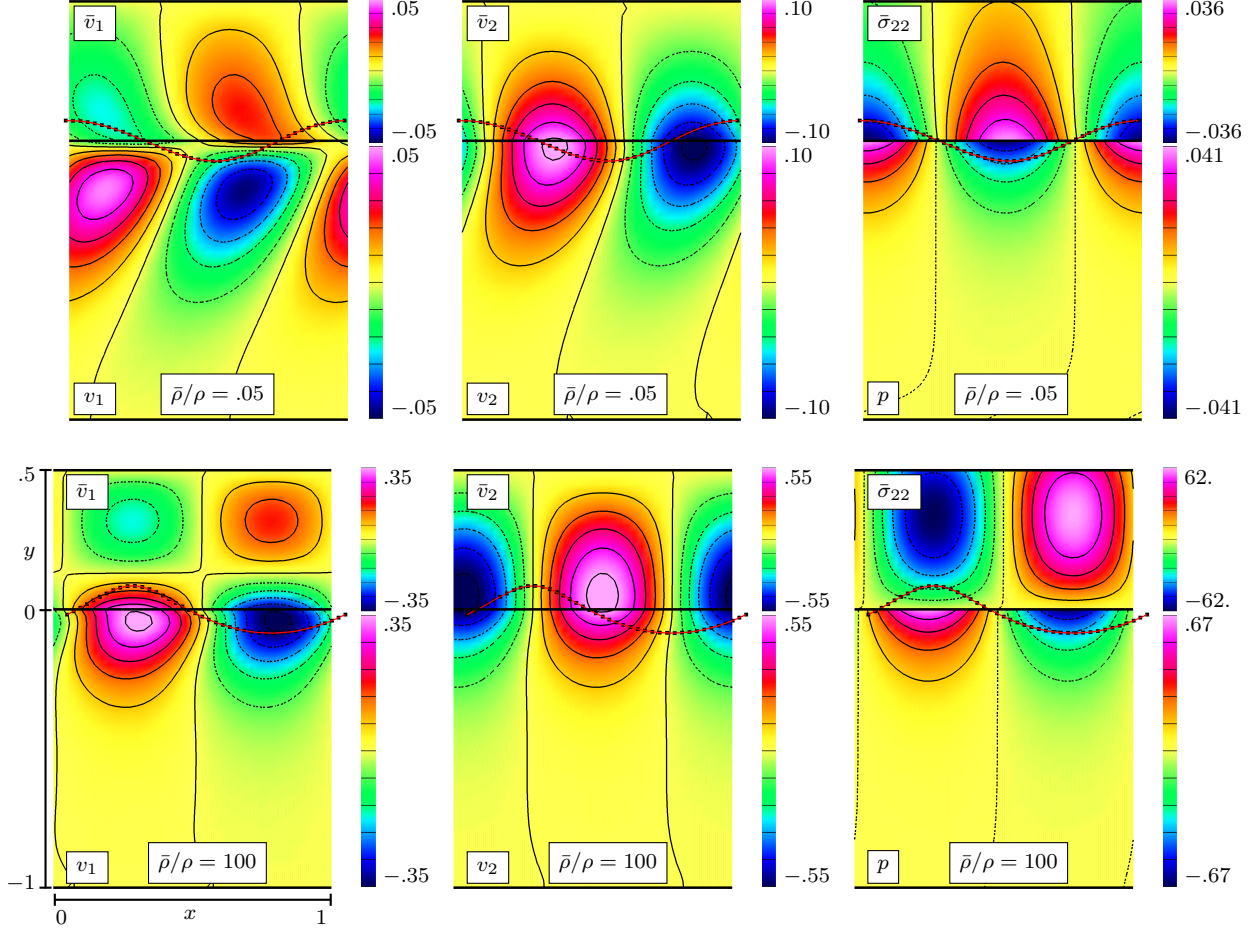


Figure 4: Traveling wave solution for a viscous incompressible fluid and elastic solid, model problem MP-VE, at $t = 0.5$. Top row: shaded contours of the computed solution for $\delta = \bar{\rho}/\rho = .05$. Bottom row: shaded contours for $\delta = \bar{\rho}/\rho = 100$. The deformed interface is shown superimposed as a curve.

Figure 4 shows shaded contour plots of the computed solution for model problem MP-VE with two different density ratios at time $t = 0.5$. The fluid viscosity is $\mu = .02$ for both cases. The shaded contours in the upper solid domain show the behavior of the velocity components, \bar{v}_1 and \bar{v}_2 , and the stress component, $\bar{\sigma}_{22}$, while the shaded contours in the lower fluid domain show the corresponding behavior of the velocity components, v_1 and v_2 , and the pressure, p . The position of the displaced interface given by the computed solid displacement, $\bar{\mathbf{u}}_1^n$ at $y_i = 0$ and $t^n = 0.5$, is shown in the plots as a curve superimposed on the shaded contours. For the light solid case with $\delta = \bar{\rho}/\rho = .05$, the corresponding exact solution has wave number $k = 2\pi$ and (complex) frequency $\omega \approx (1.290, -.5899)$, while $\omega \approx (6.714, -6.359e-3)$ for the heavy solid case with $\delta = 100$. The behavior of the solution shows an oscillation in the x direction, as expected, and decay in the y direction away from the interface at $y = 0$. It can be observed that the contour plots of the velocity components indicate that the velocity is continuous across the interface at $y = 0$ in agreement with the interface condition in (6). A further verification of the interface conditions in (6) and (7) is given in Figure 5. The plots in this figure show the behavior of the components of velocity and normal stress along the line $x = 2/3$ for the density ratios $\delta = .05$ (left) and $\delta = 100$ (right). Note that each fluid-solid component pair is continuous at $y = 0$ in agreement with the interface conditions.

Traveling wave solutions computed using the AMP algorithm may be compared with the corresponding exact solutions to further verify the stability and accuracy of the scheme. We consider the FSI model problems, MP-IA, MP-VA and MP-VE, for four different density ratios, $\delta = 10^3, 1, 10^{-1}$ and 10^{-3} . The wave number is taken to be $k = 2\pi$ for each case, and the corresponding values of ω for the exact solutions are given in Figure 6. Note that for $\delta = 10^{-3}$ a smaller value of the fluid viscosity is used in order to

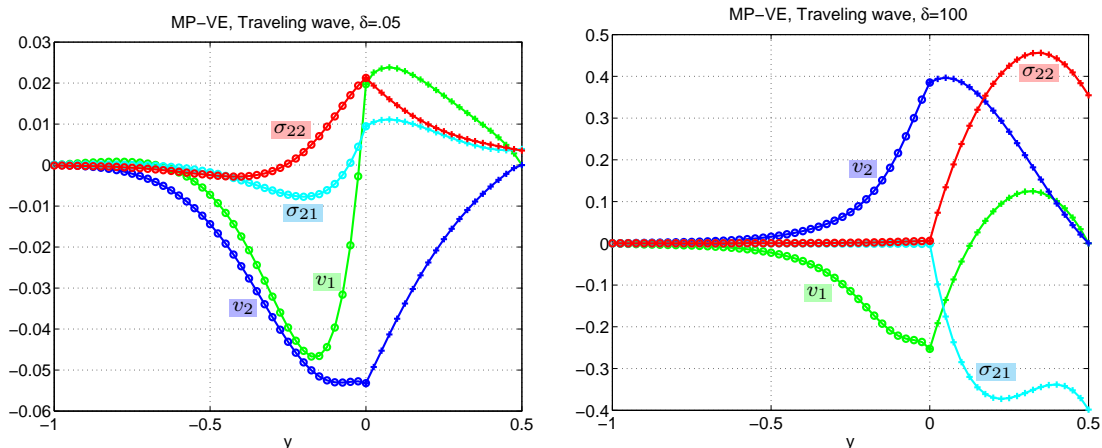


Figure 5: Plots of the computed solution along the line $x = 2/3$ for the traveling wave solution and model problem MP-VE, for $\delta = 0.05$ (left) and $\delta = 100$ (right). The fluid solution is in the interval $y \in [-1, 0]$ while the solid occupies $y \in [0, .5]$. For the right-hand plot, σ_{21} and σ_{22} are scaled by factors of 50 and 100, respectively. These plots correspond to the solutions shown in Figure 4.

Traveling wave frequencies ω			
δ	MP-IA	MP-VA	MP-VE
10^{-3}	(15.392, 0)	(.2344, -.1427)	(1.568, -0.1208)
10^{-1}	(15.513, 0)	(2.792, -0.7469)	(1.905, -0.6524)
1	(16.556, 0)	(8.126, -0.7261)	(5.082, -0.4619)
10^3	(29.294, 0)	(12.163, -9.730e-4)	(6.731, -6.365e-4)

Figure 6: Values of the (complex) frequency $\omega = a + ib = (a, b)$ for the exact traveling wave solution used in the numerical simulations of the three model problems for $k = 2\pi$, and the parameters $\rho = 1$, $H = 1$, $\bar{\lambda} = \bar{\mu} = \bar{\rho} = \delta$ and $\bar{H} = 1/2$. For the models with a viscous fluid, $\mu = .02$ for $\delta = 10^3, 1$ and 10^{-1} , while $\mu = .005$ for $\delta = 10^{-3}$.

obtain a valid traveling wave solution. The numerical solutions and corresponding maximum-norm errors are computed for a sequence of decreasing grid spacings, as was done previously in Section 8.1, and the convergence rates for the solution components are estimated.

The results of this convergence study are given in Figures 7, 8 and 9 for the model problems MP-IA, MP-VA and MP-VE, respectively. For the case of an inviscid fluid and acoustic solid supporting vertical motion only (MP-IA), the comparison between the computed solutions and the exact solutions is made at $t = 1.0$. The results show that the scheme is stable and close to second-order accurate in the maximum-norm. Since the viscosity is zero for this model problem and the discretization of the fluid equations uses central finite differences, a small amount of artificial dissipation, proportional to h_j^2 , is added to the fluid momentum equation in order to smooth any boundary layers in the error that would otherwise degrade the maximum-norm convergence rates to a small degree (the scheme is stable without dissipation). The artificial dissipation has the standard form, $a_d(\mathbf{v}_{i_1+1, i_2} + \mathbf{v}_{i_1-1, i_2} + \mathbf{v}_{i_1, i_2+1} + \mathbf{v}_{i_1, i_2-1} - 4\mathbf{v}_i)$, where a value of $a_d = 1$ is used. This term, which formally does not change the order of accuracy, is added to the right-hand side of the momentum equation. For the viscous-fluid cases (MP-VA and MP-VE) with $\mu > 0$, solutions decay in time and the comparison is made at $t = 0.3$. For both of these cases, one with an acoustic solid supporting vertical motion only and the other with a compressible elastic solid allowing motion in both directions, the results show that the AMP algorithm is stable and close to second-order accurate in the maximum-norm.

8.3. Traditional partitioned scheme

The table in Figure 10 indicates the stability of the traditional partitioned (TP) algorithm for the model problem MP-VE for different values of $\delta = \bar{\rho}/\rho$. The stability was determined experimentally by integrating

MP-IA, traveling wave, inviscid fluid, heavy acoustic solid, $\delta = 10^3$										
h_j	$E_j^{(p)}$	r	$E_j^{(v)}$	r	$E_j^{(\bar{u})}$	r	$E_j^{(\bar{v})}$	r	$E_j^{(\bar{\sigma})}$	r
1/20	8.7e0		2.2e0		6.3e-2		1.8e0		2.9e3	
1/40	3.0e0	2.9	7.5e-1	2.9	2.2e-2	2.9	6.5e-1	2.8	9.7e2	3.0
1/80	7.0e-1	4.3	1.7e-1	4.4	5.6e-3	4.0	1.6e-1	4.0	2.4e2	4.0
1/160	1.6e-1	4.4	3.8e-2	4.5	1.4e-3	4.1	3.8e-2	4.2	6.0e1	4.1
rate	1.94		1.96		1.86		1.87		1.88	

MP-IA, traveling wave, inviscid fluid, medium acoustic solid, $\delta = 1$										
h_j	$E_j^{(p)}$	r	$E_j^{(v)}$	r	$E_j^{(\bar{u})}$	r	$E_j^{(\bar{v})}$	r	$E_j^{(\bar{\sigma})}$	r
1/20	3.3e-1		1.6e-1		1.7e-2		2.6e-1		3.5e-1	
1/40	8.9e-2	3.7	4.5e-2	3.6	4.9e-3	3.6	7.1e-2	3.8	1.0e-1	3.4
1/80	2.2e-2	4.0	1.1e-2	3.9	1.2e-3	3.9	1.8e-2	3.9	3.1e-2	3.4
1/160	5.3e-3	4.2	2.9e-3	4.0	3.1e-4	4.0	4.8e-3	3.8	8.8e-3	3.5
rate	1.99		1.94		1.94		1.93		1.77	

MP-IA, traveling wave, inviscid fluid, light acoustic solid, $\delta = 10^{-1}$										
h_j	$E_j^{(p)}$	r	$E_j^{(v)}$	r	$E_j^{(\bar{u})}$	r	$E_j^{(\bar{v})}$	r	$E_j^{(\bar{\sigma})}$	r
1/20	2.5e-1		1.4e-1		1.2e-1		1.9e0		2.5e-1	
1/40	5.9e-2	4.2	3.3e-2	4.2	2.9e-2	4.2	4.5e-1	4.2	5.9e-2	4.2
1/80	1.5e-2	4.0	8.2e-3	4.1	7.6e-3	3.9	1.2e-1	3.9	1.5e-2	4.0
1/160	3.7e-3	4.0	2.1e-3	3.9	1.9e-3	4.0	3.0e-2	3.9	3.7e-3	4.0
rate	2.02		2.01		2.00		1.99		2.02	

MP-IA, traveling wave, inviscid fluid, very light acoustic solid, $\delta = 10^{-3}$										
h_j	$E_j^{(p)}$	r	$E_j^{(v)}$	r	$E_j^{(\bar{u})}$	r	$E_j^{(\bar{v})}$	r	$E_j^{(\bar{\sigma})}$	r
1/20	2.5e-1		1.1e-1		12.1e0		18.4e1		2.5e-1	
1/40	5.7e-2	4.4	2.0e-2	5.5	2.9e0	4.2	43.8e0	4.2	5.7e-2	4.4
1/80	1.4e-2	4.0	5.2e-3	3.8	7.3e-1	3.9	11.5e0	3.8	1.4e-2	4.0
1/160	3.6e-3	3.9	1.5e-3	3.5	1.9e-1	3.9	3.0e0	3.9	3.6e-3	3.9
rate	2.03		2.06		2.00		1.98		2.03	

Figure 7: Traveling wave solution for an inviscid incompressible fluid and acoustic solid (model problem MP-IA). Maximum errors and estimated convergence rates at $t = 1.0$, computed using the AMP scheme for a heavy solid, $\delta = 10^3$, medium solid, $\delta = 1$, light solid, $\delta = 10^{-1}$ and very light solid $\delta = 10^{-3}$.

the equations for a large number of time steps, and looking for exponential blowup. For heavy enough solids one might expect the TP algorithm to be stable. However, from the theory for the model problem discussed in Section 6 (see Theorem 4), it was shown that the scheme becomes unstable on a sufficiently fine grid, for any value of δ no matter how large. For a given ratio δ , the scheme may be stable on a coarse grid but becomes unstable for all sufficiently fine grids. The question is whether a similar result holds for the more general model problem MP-VE. The results in Figure 10 strongly suggest that this behavior also holds for the more complex model problem. For $\delta = \bar{\rho}/\rho = 100$ the scheme is stable for $h_j = 1/20$ but unstable for $h_j = 1/40$ and smaller. For a larger ratio, $\delta = 200$, the scheme is stable for $h_j = 1/20$ and $h_j = 1/40$ but unstable for $h_j = 1/180$ and smaller. This trend continues.

9. Conclusions

In Part I of this two-part paper, we have described a stable added-mass partitioned (AMP) algorithm for coupling incompressible flows with compressible elastic solids. The AMP algorithm is apparently the first stable partitioned scheme for incompressible flows and compressible elastic bulk solids that does not require any sub-iterations per time step. The Robin interface conditions for the AMP approach are derived from a local characteristic decomposition in the solid, and these define relationships between the fluid velocity and traction on the interface in terms of the outgoing characteristic in the solid. For fractional-step incompressible flow algorithms, such as the one used in this paper, an alternative Robin interface condition was derived that defines a mixed boundary condition on the pressure; this can be used when solving the pressure equation. A

MP-VA, traveling wave, viscous fluid, $\mu = .02$, heavy acoustic solid, $\delta = 10^3$										
h_j	$E_j^{(p)}$	r	$E_j^{(v)}$	r	$E_j^{(\bar{u})}$	r	$E_j^{(\bar{v})}$	r	$E_j^{(\bar{\sigma})}$	r
1/20	2.9e-1		1.5e-1		2.1e-3		2.1e-2		3.3e1	
1/40	8.5e-2	3.3	4.1e-2	3.6	5.0e-4	4.3	4.8e-3	4.5	7.5e0	4.4
1/80	1.5e-2	5.8	7.7e-3	5.3	1.2e-4	4.1	1.1e-3	4.2	1.8e0	4.2
1/160	2.0e-3	7.2	1.4e-3	5.4	3.9e-5	3.1	3.7e-4	3.1	5.7e-1	3.2
rate	2.40		2.25		1.94		1.96		1.96	

MP-VA, traveling wave, viscous fluid, $\mu = .02$, medium acoustic solid, $\delta = 1$										
h_j	$E_j^{(p)}$	r	$E_j^{(v)}$	r	$E_j^{(\bar{u})}$	r	$E_j^{(\bar{v})}$	r	$E_j^{(\bar{\sigma})}$	r
1/20	5.4e-2		4.8e-2		3.2e-3		3.6e-2		7.7e-2	
1/40	1.1e-2	4.8	1.1e-2	4.4	8.4e-4	3.9	9.3e-3	3.9	1.8e-2	4.4
1/80	2.3e-3	4.8	2.3e-3	4.8	2.0e-4	4.2	2.2e-3	4.3	4.0e-3	4.4
1/160	5.5e-4	4.2	5.2e-4	4.3	4.9e-5	4.0	5.2e-4	4.1	1.1e-3	3.7
rate	2.21		2.18		2.02		2.05		2.07	

MP-VA, traveling wave, viscous fluid, $\mu = .02$, light acoustic solid, $\delta = 10^{-1}$										
h_j	$E_j^{(p)}$	r	$E_j^{(v)}$	r	$E_j^{(\bar{u})}$	r	$E_j^{(\bar{v})}$	r	$E_j^{(\bar{\sigma})}$	r
1/20	2.5e-3		8.3e-3		2.1e-3		8.3e-3		6.2e-3	
1/40	6.2e-4	4.0	1.9e-3	4.3	5.3e-4	3.9	1.9e-3	4.3	1.3e-3	4.6
1/80	1.6e-4	4.0	4.2e-4	4.5	1.3e-4	4.2	4.2e-4	4.5	2.9e-4	4.6
1/160	4.0e-5	3.9	9.8e-5	4.3	3.0e-5	4.2	9.8e-5	4.3	6.9e-5	4.2
rate	1.99		2.14		2.04		2.14		2.16	

MP-VA, traveling wave, viscous fluid, $\mu = .005$, very light acoustic solid, $\delta = 10^{-3}$										
h_j	$E_j^{(p)}$	r	$E_j^{(v)}$	r	$E_j^{(\bar{u})}$	r	$E_j^{(\bar{v})}$	r	$E_j^{(\bar{\sigma})}$	r
1/20	2.7e-5		3.2e-4		1.5e-3		6.2e-3		2.7e-5	
1/40	7.2e-6	3.7	8.6e-5	3.7	2.5e-4	6.2	1.6e-3	4.0	5.9e-6	4.5
1/80	1.9e-6	3.9	2.1e-5	4.1	3.4e-5	7.3	3.5e-4	4.5	1.2e-6	4.9
1/160	4.5e-7	4.2	5.1e-6	4.1	4.0e-6	8.6	7.7e-5	4.5	2.5e-7	4.8
rate	1.96		1.99		2.87		2.11		2.25	

Figure 8: Traveling wave solution for an viscous incompressible fluid and acoustic solid (model problem MP-VA). Maximum errors and estimated convergence rates at $t = 0.3$, computed using the AMP scheme for a heavy solid, $\delta = 10^3$, medium solid, $\delta = 1$, light solid, $\delta = 10^{-1}$, and very light solid $\delta = 10^{-3}$.

comparison of the Robin interface conditions derived here for the case of compressible bulk solids and those suitable for FSI problems involving elastic shells described in Part II is given in [4].

A normal mode analysis for a model FSI problem showed that the AMP algorithm is stable even for very light solids when the added-mass effects are large. An analysis of a traditional partitioned algorithm showed that the scheme is, in fact, formally unconditionally unstable for any ratio of the solid to fluid density, no matter how large. The traditional scheme may be stable on a coarse grid but becomes unstable for a sufficiently fine grid.

We derived exact traveling wave solutions for a number of FSI model problems and these were used to verify the stability and accuracy of the AMP algorithm. Numerical results confirmed that the AMP scheme was stable for light, medium and heavy solids, and the scheme was second-order accurate in the maximum-norm. The traveling wave solutions obtained here would also be useful in evaluating other FSI algorithms.

The AMP algorithm was described for the case of FSI problems with small perturbations in the solution with respected to a fixed interface position. In future work, we plan to incorporate the AMP approximations into our deforming composite grid framework [2] that solves the full three-dimensional and nonlinear incompressible Navier-Stokes equations and that supports large structural deformations.

MP-VE, traveling wave, viscous fluid, $\mu = .02$, heavy elastic solid, $\delta = 10^3$										
h_j	$E_j^{(p)}$	r	$E_j^{(v)}$	r	$E_j^{(\bar{u})}$	r	$E_j^{(\bar{v})}$	r	$E_j^{(\bar{\sigma})}$	r
1/20	1.2e-2		1.9e-2		2.4e-3		1.6e-2		3.5e1	
1/40	2.9e-3	4.1	3.7e-3	5.1	4.5e-4	5.4	3.1e-3	5.2	9.1e0	3.9
1/80	6.5e-4	4.5	6.0e-4	6.1	8.3e-5	5.4	6.0e-4	5.1	2.5e0	3.6
1/160	1.5e-4	4.3	1.3e-4	4.8	1.6e-5	5.0	1.2e-4	4.8	6.8e-1	3.7
rate	2.18		2.21		2.03		2.03		1.95	

MP-VE, traveling wave, viscous fluid, $\mu = .02$, medium elastic solid, $\delta = 1$										
h_j	$E_j^{(p)}$	r	$E_j^{(v)}$	r	$E_j^{(\bar{u})}$	r	$E_j^{(\bar{v})}$	r	$E_j^{(\bar{\sigma})}$	r
1/20	1.3e-2		1.2e-2		2.6e-3		9.2e-3		4.4e-2	
1/40	2.6e-3	5.0	2.7e-3	4.3	5.9e-4	4.4	2.2e-3	4.2	8.5e-3	5.2
1/80	4.8e-4	5.5	5.6e-4	4.8	1.3e-4	4.6	5.0e-4	4.3	1.7e-3	5.0
1/160	9.4e-5	5.1	1.2e-4	4.5	2.9e-5	4.5	1.2e-4	4.3	4.1e-4	4.2
rate	2.39		2.19		2.17		2.10		2.26	

MP-VE, traveling wave, viscous fluid, $\mu = .02$, light elastic solid, $\delta = 10^{-1}$										
h_j	$E_j^{(p)}$	r	$E_j^{(v)}$	r	$E_j^{(\bar{u})}$	r	$E_j^{(\bar{v})}$	r	$E_j^{(\bar{\sigma})}$	r
1/20	3.3e-3		5.4e-3		1.5e-3		5.8e-3		2.0e-3	
1/40	7.0e-4	4.7	1.2e-3	4.4	3.9e-4	3.9	1.4e-3	4.2	4.0e-4	5.0
1/80	1.4e-4	4.9	2.7e-4	4.6	8.8e-5	4.4	3.0e-4	4.6	8.3e-5	4.8
1/160	3.0e-5	4.7	6.0e-5	4.4	2.0e-5	4.4	6.6e-5	4.4	2.9e-5	2.9
rate	2.26		2.16		2.08		2.16		2.06	

MP-VE, traveling wave, viscous fluid, $\mu = .005$, very light elastic solid, $\delta = 10^{-3}$										
h_j	$E_j^{(p)}$	r	$E_j^{(v)}$	r	$E_j^{(\bar{u})}$	r	$E_j^{(\bar{v})}$	r	$E_j^{(\bar{\sigma})}$	r
1/20	2.1e-5		3.2e-4		8.0e-4		2.4e-3		1.3e-5	
1/40	4.6e-6	4.6	9.2e-5	3.4	1.6e-4	4.9	5.8e-4	4.2	3.4e-6	3.9
1/80	9.8e-7	4.7	2.3e-5	4.0	2.7e-5	6.1	10.0e-5	5.8	1.1e-6	3.2
1/160	2.2e-7	4.5	5.7e-6	4.0	4.3e-6	6.3	2.2e-5	4.6	2.9e-7	3.6
rate	2.21		1.93		2.53		2.29		1.82	

Figure 9: Traveling wave solution for a viscous incompressible fluid and elastic solid (model problem MP-VE). Maximum errors and estimated convergence rates at $t = 0.3$, computed using the AMP scheme for a heavy solid, $\delta = 10^3$, medium solid, $\delta = 1$, light solid, $\delta = 10^{-1}$, and very light solid $\delta = 10^{-3}$.

MP-VE, traveling wave, TP algorithm				
h_j	$\delta = 800$	$\delta = 400$	$\delta = 200$	$\delta = 100$
1/20	stable	stable	stable	stable
1/40	stable	stable	stable	unstable
1/80	stable	stable	unstable	unstable
1/160	stable	unstable	unstable	unstable
1/320	unstable	unstable	unstable	unstable

Figure 10: Stability of the traditional partitioned (TP) algorithm for the traveling wave solution for model problem MP-VE for different values of $\delta = \bar{\rho}/\rho$ with $\rho = 1$. As predicted by the theory, for any given value of δ , no matter how large, the TP algorithm becomes unstable when the mesh is sufficiently fine.

Appendix A. Traveling wave exact solutions for the FSI model problems

In this section we present exact *traveling wave* solutions to the three FSI model problems MP-IA, MP-VA and MP-VE defined in Section 4. In each case we look for traveling wave solutions of the form

$$\mathbf{v}(x, y, t) = \hat{\mathbf{v}}(y) e^{i(kx - \omega t)}, \quad p(x, y, t) = \hat{p}(y) e^{i(kx - \omega t)}, \quad \bar{\mathbf{u}}(x, y, t) = \hat{\mathbf{u}}(y) e^{i(kx - \omega t)}, \quad (\text{A.1})$$

for the fluid velocity, fluid pressure and solid displacement, respectively. The solutions are assumed to be periodic in the horizontal coordinate x with wave number k , and have frequency ω (possibly complex) in time t . Since the fundamental period in the horizontal direction is L we are interested in values of k that

are integer multiples of $2\pi/L$. After substituting these forms into the governing equations, the result is a system of ordinary differential equations for $\hat{\mathbf{v}}(y)$, $\hat{p}(y)$ and $\hat{\mathbf{u}}(y)$ in terms of the vertical coordinate y subject to homogeneous boundary and interface conditions. This system has non-trivial solutions (eigenfunctions) provided ω and k are solutions of a certain determinant condition which defines the dispersion relation for each model problem.

For the fluid solutions it is helpful to define

$$C_k = \cosh(kH), \quad S_k = \sinh(kH), \quad C_\alpha = \cosh(\alpha H), \quad S_\alpha = \sinh(\alpha H),$$

where

$$\alpha^2 = k^2 - \frac{i\rho\omega}{\mu}.$$

For the solid solutions we define

$$C_a = \cosh(a\bar{H}), \quad S_a = \sinh(a\bar{H}), \quad C_b = \cosh(b\bar{H}), \quad S_b = \sinh(b\bar{H}),$$

where

$$a^2 = k^2 - \frac{\omega^2}{\bar{c}_p^2}, \quad b^2 = k^2 - \frac{\omega^2}{\bar{c}_s^2}.$$

Appendix A.1. Traveling wave solution for MP-IA

Solutions of the system of ODEs and boundary conditions at $y = -H$ and $y = \bar{H}$ for the MP-IA model problem can be written in the form

$$\begin{aligned} \hat{v}_1(y) &= iA_f \cosh(k(y+H)), & \hat{v}_2(y) &= A_f \sinh(k(y+H)), \\ \hat{p}(y) &= \frac{i\rho\omega}{k} A_f \cosh(k(y+H)), & \hat{u}_2(y) &= A_s \sinh(a(y-\bar{H})), \end{aligned} \tag{A.2}$$

where A_f and A_s are constants. Application of the interface conditions at $y = 0$ gives the matrix problem

$$M_{\text{IA}} \begin{bmatrix} A_f \\ A_s \end{bmatrix} = \begin{bmatrix} S_k & -i\omega S_a \\ i\rho\omega C_k & \bar{\rho}\bar{c}_p^2 a k C_a \end{bmatrix} \begin{bmatrix} A_f \\ A_s \end{bmatrix} = 0.$$

For non-trivial solutions we require values of ω and k for which $\det(M_{\text{IA}}) = 0$. This condition leads to the dispersion relation,

$$W_{\text{IA}}(\omega, k) = \bar{\rho}\bar{c}_p^2 a k S_k C_a - \rho\omega^2 C_k S_a = 0. \tag{A.3}$$

Given a solution of (A.3) for ω and k (usually values for $k \in \mathbb{R}$ and the other parameters are specified, and then (A.3) becomes a nonlinear equation for ω), A_f can be determined in terms of the free parameter A_s as

$$A_f = i\omega \frac{S_a}{S_k} A_s.$$

We choose A_s so that the maximum displacement of the interface is equal to the real-valued amplitude parameter \bar{u}_{max} , i.e., $|\hat{u}_2(0)| = \bar{u}_{\text{max}}$. The real and imaginary parts of the solutions in (A.1) with component coefficient functions given in (A.2) define real solutions to the model problem MP-IA.

An analysis of the dispersion relation in (A.3) shows that there is a plus-minus pair of real solutions for ω satisfying $0 < |\omega| < \bar{c}_p |k|$ if $\bar{\rho}/\rho < (k\bar{H}) \coth(kH)$, and there are an infinite number of real plus-minus pairs satisfying $|\omega| > \bar{c}_p |k|$. In the limit of large $|\omega|$, it can be shown that these solutions have the asymptotic form $\omega \sim \pm n\pi\bar{c}_p/\bar{H}$ for large integers n . For example, if $k = 2\pi$, $\bar{\rho} = \bar{\lambda} = \bar{\mu} = 0.1$, $\bar{H} = 0.5$, $\rho = 1$ and $H = 1$, then $\omega \approx 3.36460699$ is the one positive solution satisfying $0 < |\omega| < \bar{c}_p |k|$, while $\omega \approx 15.5134370$ is the smallest positive solution satisfying $|\omega| > \bar{c}_p |k|$.

Appendix A.2. Traveling wave solution for MP-VA

Solution of the system of ODEs and boundary conditions at $y = H$ for the viscous fluid domain of the model problem MP-VA can be written in the form

$$\begin{aligned}
\hat{v}_1(y) &= iA_f \left(kS_\alpha \cosh(ky) + \mathcal{D} \cosh(k(y+H)) - \alpha S_k \cosh(\alpha y) \right) \\
&\quad + \frac{i\alpha B_f}{k} \left(kS_\alpha \cosh(ky) + \mathcal{D} \cosh(\alpha(y+H)) - \alpha S_k \cosh(\alpha y) \right), \\
\hat{v}_2(y) &= A_f \left(kS_\alpha \sinh(ky) + \mathcal{D} \sinh(k(y+H)) - kS_k \sinh(\alpha y) \right), \\
&\quad + B_f \left(\alpha S_\alpha \sinh(ky) + \mathcal{D} \sinh(\alpha(y+H)) - \alpha S_k \sinh(\alpha y) \right), \\
\hat{p}(y) &= \frac{i\rho\omega}{k} \left[A_f \left(kS_\alpha \cosh(ky) + \mathcal{D} \cosh(k(y+H)) \right) + B_f \alpha S_\alpha \cosh(ky) \right],
\end{aligned} \tag{A.4}$$

where

$$\mathcal{D} = \alpha C_\alpha S_k - k C_k S_\alpha,$$

and A_f and B_f are constants to be determined. Solutions of the system of ODEs and the boundary condition at $y = -\bar{H}$ for the solid domain can be taken as $\hat{u}_2(y)$ in (A.2) with constant A_s to be determined.

The three constants A_f , B_f and A_s are determined by the three interface conditions for MP-VA. These leads to the matrix equation

$$M_{VA} \begin{bmatrix} A_f \\ B_f \\ A_s \end{bmatrix} = 0,$$

where $M_{VA} = [m_{ij}] \in \mathbb{C}^{3 \times 3}$ with

$$\begin{aligned}
m_{11} &= i(kS_\alpha - \alpha S_k + \mathcal{D}C_k), & m_{12} &= \frac{i}{k}\alpha(kS_\alpha - \alpha S_k + \mathcal{D}C_\alpha), & m_{13} &= 0, \\
m_{21} &= \mathcal{D}S_k, & m_{22} &= \mathcal{D}S_\alpha, & m_{23} &= -i\omega S_a, \\
m_{31} &= i\rho \frac{\omega}{k}(kS_\alpha + \mathcal{D}C_k) - 2\mu(k^2 S_\alpha - k\alpha S_k + \mathcal{D}kC_k), \\
m_{32} &= i\rho \frac{\omega}{k}\alpha S_\alpha - 2\mu(\alpha k S_\alpha - \alpha^2 S_k + \mathcal{D}\alpha C_\alpha), \\
m_{33} &= \bar{\rho} \bar{c}_p^2 a C_a.
\end{aligned}$$

For nontrivial solutions we require $\det(M_{VA}) = 0$, which leads to the dispersion relation

$$W_{VA}(\omega, k) = \det(M_{VA}) = 0. \tag{A.5}$$

The precise form for $W_{VA}(\omega, k)$ is messy and not particularly revealing, and so we suppress the details here. (The form can be found readily using the given components of M_{VA} and the symbolic program Maple, for example, and then solved numerically.) Once a solution (ω, k) is found, the constants A_f , B_f can be determined in terms of A_s from

$$\begin{bmatrix} m_{11} & m_{12} \\ m_{21} & m_{22} \end{bmatrix} \begin{bmatrix} A_f \\ B_f \end{bmatrix} = -A_s \begin{bmatrix} m_{13} \\ m_{23} \end{bmatrix}.$$

The parameter A_s is an arbitrary constant and can be chosen, for example, so that $|\hat{u}_2(0)| = \bar{u}_{\max}$.

For the dispersion relation in (A.5) we have investigated solutions numerically. For a chosen set of parameters of the problem, it appears that there are an infinite number of complex-valued solutions for ω . For example, if $k = 2\pi$, $\bar{\rho} = \bar{\lambda} = \bar{\mu} = 0.1$, $\bar{H} = 0.5$, $\rho = 1$, $\mu = .02$ and $H = 1$, then one solution is given by the complex number $\omega \approx (2.79247701, -0.746859802)$.

Appendix A.3. Traveling wave solution for MP-VE

For the case of the model problem MP-VE we use the solutions in (A.4) for the fluid. As noted earlier, these functions satisfy the system of ODEs in the fluid and the boundary condition at $y = H$. For the elastic solid, we use

$$\begin{aligned}\hat{u}_1 &= A_s \left(-k^2 S_b \cosh(ay) + \bar{\mathcal{D}} \cosh(a(y - \bar{H})) + abS_a \cosh(by) \right) \\ &\quad + B_s \left(-k^2 S_b \cosh(ay) + \bar{\mathcal{D}} \cosh(b(y - \bar{H})) + abS_a \cosh(by) \right), \\ \hat{u}_2 &= \frac{aA_s}{ik} \left(-k^2 S_b \sinh(ay) + \bar{\mathcal{D}} \sinh(a(y - \bar{H})) + k^2 S_a \sinh(by) \right) \\ &\quad + \frac{kB_s}{ib} \left(-abS_b \sinh(ay) + \bar{\mathcal{D}} \sinh(b(y - \bar{H})) + abS_a \sinh(by) \right),\end{aligned}\tag{A.6}$$

where

$$\bar{\mathcal{D}} = k^2 C_a S_b - abC_b S_a.$$

The four constants A_f , B_f , A_s and B_s are determined by the four interface conditions. These leads to the matrix equation

$$M_{\text{VE}} \begin{bmatrix} A_f \\ B_f \\ A_s \\ B_s \end{bmatrix} = 0,$$

where $M_{\text{VE}} = [m_{ij}] \in \mathbb{C}^{4 \times 4}$ has components

$$\begin{aligned}m_{11} &= i(kS_\alpha - \alpha S_k + \mathcal{D}C_k), & m_{12} &= i\alpha(kS_\alpha - \alpha S_k + \mathcal{D}C_\alpha)/k, \\ m_{13} &= i\omega(-k^2 S_b/\bar{\mathcal{D}} + C_a + abS_a/\bar{\mathcal{D}}), & m_{14} &= i\omega(-k^2 S_b/\bar{\mathcal{D}} + abS_a/\bar{\mathcal{D}} + C_b), \\ m_{21} &= \mathcal{D}S_k, & m_{22} &= \mathcal{D}S_\alpha, & m_{23} &= -\omega a S_a/k, & m_{24} &= -\omega k S_b/b, \\ m_{31} &= -2i\mu k \mathcal{D}S_k, & m_{32} &= -\mu(i\alpha^2 \mathcal{D}S_\alpha/k + ik \mathcal{D}S_\alpha), & m_{33} &= -2\bar{\mu} a S_a, & m_{34} &= \bar{\mu}(-bS_b - k^2 S_b/b), \\ m_{41} &= i\rho\omega(kS_\alpha + \mathcal{D}C_k)/k - 2\mu(k^2 S_\alpha - k\alpha S_k + \mathcal{D}kC_k), & m_{42} &= i\rho\omega\alpha S_\alpha/k - 2\mu(\alpha k S_\alpha - \alpha^2 S_k + \mathcal{D}\alpha C_\alpha), \\ m_{43} &= -i(\bar{\lambda} + 2\bar{\mu})(-a^2 k S_b/\bar{\mathcal{D}} + a^2 C_a/k + kabS_a/\bar{\mathcal{D}}) + i\bar{\lambda}k(-k^2 S_b/\bar{\mathcal{D}} + C_a + abS_a/\bar{\mathcal{D}}), \\ m_{44} &= -i(\bar{\lambda} + 2\bar{\mu})(-a^2 k S_b/\bar{\mathcal{D}} + kabS_a/\bar{\mathcal{D}} + kC_b) + i\bar{\lambda}k(-k^2 S_b/\bar{\mathcal{D}} + abS_a/\bar{\mathcal{D}} + C_b).\end{aligned}$$

Non-trivial solutions are obtained if ω and k satisfy the dispersion relation

$$W_{\text{VE}}(\omega, k) = \det(M_{\text{VE}}) = 0.$$

For a given solution of $W_{\text{VE}}(\omega, k) = 0$, the constants A_f , B_f , A_s can be defined in terms of B_s from

$$\begin{bmatrix} m_{11} & m_{12} & m_{13} \\ m_{21} & m_{22} & m_{23} \\ m_{31} & m_{32} & m_{33} \end{bmatrix} \begin{bmatrix} A_f \\ B_f \\ A_s \end{bmatrix} = -B_s \begin{bmatrix} m_{14} \\ m_{24} \\ m_{34} \end{bmatrix}.$$

In this construction, the parameter B_s is an arbitrary constant. We choose B_s so that the maximum displacement of the interface is \bar{u}_{max} , i.e. $|\hat{\mathbf{u}}(0)| = \sqrt{\hat{u}_1^2(0) + \hat{u}_2^2(0)} = \bar{u}_{\text{max}}$. The real and imaginary parts of (A.1) with (A.4) and (A.6) define real solutions to the model problem MP-VE.

As in the previous case, we investigate solutions of $W_{\text{VE}}(\omega, k) = 0$ numerically. For example, if $k = 2\pi$, $\bar{\rho} = \bar{\lambda} = \bar{\mu} = 0.1$, $\bar{H} = 0.5$, $\rho = 1$, $\mu = .02$ and $H = 1$, then one solution is given by $\omega \approx (1.90532196, -0.652436711)$.

Appendix B. AMP time-stepping procedures

This section provides partial implementations of some of the procedures that appear in the AMP algorithm described in Section 7. Let ∇_h and Δ_h denote discrete approximations to the operators ∇ and

Δ , respectively, and let \mathbf{L}_i^n be the discretized form of the right-hand-side to the fluid momentum equation defined by

$$\mathbf{L}_i^n \equiv -\frac{1}{\rho} \nabla_h p_i^n + \frac{\mu}{\rho} \Delta_h \mathbf{v}_i^n. \quad (\text{B.1})$$

Let Ω_h^F denote the set of grid point indices, \mathbf{i} , corresponding to the interior, boundary and interface points of the fluid domain. Similarly, let Ω_h^S denote the corresponding indices in the solid domain, and let Γ_h denote the set of indices on the interface.

Procedure 1 Advance the fluid velocity from time t^{n-1} to t^n , return a predicted velocity $\mathbf{v}_i^{(p)}$. This routine assigns interior, boundary and interface points.

- 1: **procedure** `advanceFluid`($\mathbf{v}_i^{n-1}, p_i^{n-1}, \mathbf{v}_i^{n-2}, p_i^{n-2}$)
 - 2: $\mathbf{v}_i^{(p)} = \mathbf{v}_i^{n-1} + \Delta t \left(\frac{3}{2} \mathbf{L}_i^{n-1} - \frac{1}{2} \mathbf{L}_i^{n-2} \right), \quad \mathbf{i} \in \Omega_h^F$ ▷ (Adams-Bashforth).
 - 3: **return** $\mathbf{v}_i^{(p)}$
 - 4: **end procedure**
-

Procedure 2 Advance the fluid velocity from t^{n-1} to t^n given an approximation to the state at t^n . This routine assigns interior, boundary and interface points.

- 1: **procedure** `correctFluid`($\mathbf{v}_i^{(p)}, p_i^{(p)}, \mathbf{v}_i^{n-1}, p_i^{n-1}$)
 - 2: $\mathbf{v}_i^n = \mathbf{v}_i^{n-1} + \frac{\Delta t}{2} \left(\mathbf{L}_i^{(p)} + \mathbf{L}_i^{n-1} \right), \quad \mathbf{i} \in \Omega_h^F$ ▷ (trapezoidal rule).
 - 3: **return** \mathbf{v}_i^n
 - 4: **end procedure**
-

Procedure 3 Solve for the pressure at all grid points.

- 1: **procedure** `solveFluidPressureEquation`($\mathbf{v}_i, \bar{\mathbf{v}}_i, \bar{\boldsymbol{\sigma}}_i \mathbf{n}_i, \dot{\bar{\mathbf{v}}}_i$)
 - 2: ▷ Solve the following system of equations for the pressure:
 - 3: $\Delta_h p_i = 0, \quad \mathbf{i} \in \Omega_h^F$
 - 4: $-p_i - \frac{\bar{z}_p \Delta t}{\rho} \mathbf{n}_i \cdot \nabla_h p_i = -\mathbf{n}_i^T \boldsymbol{\tau}_i \mathbf{n}_i + \frac{\mu \bar{z}_p \Delta t}{\rho} \mathbf{n}_i^T (\nabla_h \times \nabla_h \times \mathbf{v}_i) + \mathbf{n}_i^T \bar{\boldsymbol{\sigma}}_i \mathbf{n}_i + \bar{z}_p \Delta t \mathbf{n}_i^T \dot{\bar{\mathbf{v}}}_i, \quad \mathbf{i} \in \Gamma_h$
 - 5: **return** p_i
 - 6: **end procedure**
-

Notes: Line 4 is the Robin boundary condition for the pressure (26). In practice it is useful to add a divergence damping term to the right-hand-side of the the pressure equation on line 3 following [6, 7].

Procedure 4 Project the interface velocity (if $\beta = 0$ do not include traction terms).

```

1: procedure projectInterfaceVelocity(  $\mathbf{v}_i, p_i, \bar{\mathbf{v}}_i, \bar{\boldsymbol{\sigma}}_i \mathbf{n}_i, \beta$  )
2:    $\mathbf{n}_i^T \mathbf{v}_i^I = \frac{z_f}{z_f + \bar{z}_p} \mathbf{n}_i^T \mathbf{v}_i + \frac{\bar{z}_p}{z_f + \bar{z}_p} \mathbf{n}_i^T \bar{\mathbf{v}}_i + \frac{\beta}{\bar{z}_p + z_f} \left( \mathbf{n}_i^T \bar{\boldsymbol{\sigma}}_i \mathbf{n}_i + p_i - \mathbf{n}_i^T \boldsymbol{\tau}_i \mathbf{n}_i \right), \quad \mathbf{i} \in \Gamma_h$ 
3:    $\mathbf{e}_m^T \mathbf{v}_i^I = \frac{z_f}{z_f + \bar{z}_s} \mathbf{e}_m^T \mathbf{v}_i + \frac{\bar{z}_s}{z_f + \bar{z}_s} \mathbf{e}_m^T \bar{\mathbf{v}}_i + \frac{\beta}{\bar{z}_s + z_f} \left( \mathbf{e}_m^T \bar{\boldsymbol{\sigma}}_i \mathbf{n}_i - \mathbf{e}_m^T \boldsymbol{\tau}_i \mathbf{n}_i \right), \quad m = 1, 2, \quad \mathbf{i} \in \Gamma_h$ 
4:   return  $\mathbf{v}_i^I$ 
5: end procedure

```

Procedure 5 Apply the boundary conditions on the fluid velocity. Return the interface velocity and traction.

```

1: procedure assignFluidVelocityBoundaryConditions(  $\mathbf{v}_i, p_i, \mathbf{v}_i^I, \bar{\mathbf{v}}_i, \bar{\boldsymbol{\sigma}}_i \mathbf{n}_i$  )
2:    $\mathbf{v}_i = \mathbf{v}_i^I, \quad \mathbf{i} \in \Gamma_h$ 
3:   ▷ Solve the following equations to determine  $\mathbf{v}_i$  on the boundary and ghost line.
4:    $\rho \mathbf{e}_m^T (\mathbf{v}_i - \mathbf{v}_i^n) / \Delta t + (\mu/2) \mathbf{e}_m^T (\Delta_h \mathbf{v}_i + \Delta_h \mathbf{v}_i^n) = (1/2) \mathbf{e}_m^T (\nabla_h p_i + \nabla_h p_i^n), \quad \mathbf{i} \in \Gamma_h,$ 
5:    $\bar{z}_s \mathbf{e}_m^T \mathbf{v}_i + \mu \mathbf{e}_m^T (\nabla_h \mathbf{v}_i + (\nabla_h \mathbf{v}_i)^T) \mathbf{n}_i = \mathbf{e}_m^T \bar{\boldsymbol{\sigma}}_i \mathbf{n}_i + \bar{z}_s \mathbf{e}_m^T \bar{\mathbf{v}}_i, \quad \mathbf{i} \in \Gamma_h \quad \triangleright \text{(Eqn (25))}$ 
6:    $\nabla_h \cdot \mathbf{v}_i = 0, \quad \mathbf{i} \in \Gamma_h,$ 
7:   ▷ Determine the new interface values.
8:    $\mathbf{v}_i^I = \mathbf{v}_i, \quad (\boldsymbol{\sigma} \mathbf{n})_i^I = -p_i \mathbf{n}_i + \boldsymbol{\tau}_i \mathbf{n}_i, \quad \mathbf{i} \in \Gamma_h$ 
9:   return  $(\mathbf{v}_i^I, (\boldsymbol{\sigma} \mathbf{n})_i^I)$ 
10: end procedure

```

Note: When the velocity is advanced treating $\mu \Delta \mathbf{v}$ explicitly in time, the AMP boundary condition (25) (line 5) is combined with the interior equation on the boundary (line 4) to determine values on the boundary and first ghost line. This is done since for *small* \bar{z}_s , equation (25) can be thought of as primarily determining the ghost values, while for *large* \bar{z}_s equation (25) primarily sets the boundary value. When $\mu \Delta \mathbf{v}$ is treated implicitly in time, equation (25) is incorporated directly into the implicit system, to the same effect.

References

- [1] J. W. Banks, B. Sjögreen, A normal mode stability analysis of numerical interface conditions for fluid/structure interaction, *Commun. Comput. Phys.* 10 (2) (2011) 279–304, .
- [2] J. W. Banks, W. D. Henshaw, D. W. Schwendeman, Deforming composite grids for solving fluid structure problems, *J. Comput. Phys.* 231 (9) (2012) 3518 – 3547.
- [3] S. Badia, F. Nobile, C. Vergara, Fluid-structure partitioned procedures based on Robin transmission conditions, *Journal of Computational Physics* 227 (14) (2008) 7027 – 7051.
- [4] J. W. Banks, W. D. Henshaw, D. W. Schwendeman, An analysis of a new stable partitioned algorithm for FSI problems. Part II: Incompressible flow and structural shells, *J. Comput. Phys.*
- [5] B. Gustafsson, H.-O. Kreiss, J. Oliger, *Time Dependent Problems and Difference Methods*, John Wiley and Sons Inc., 1995.
- [6] W. D. Henshaw, A fourth-order accurate method for the incompressible Navier-Stokes equations on overlapping grids, *J. Comput. Phys.* 113 (1) (1994) 13–25.
- [7] M. M. Hafez (Ed.), *A Split-Step Scheme for the Incompressible Navier-Stokes Equations*, World Scientific, 2003.

- [8] D. Appelö, J. W. Banks, W. D. Henshaw, D. W. Schwendeman, Numerical methods for solid mechanics on overlapping grids: Linear elasticity, *J. Comput. Phys.* 231 (18) (2012) 6012–6050.
- [9] E. H. van Brummelen, Added mass effects of compressible and incompressible flows in fluid-structure interaction, *Journal of Applied Mechanics* 76 (2) (2009) 021206–021212.
- [10] J. W. Banks, W. D. Henshaw, B. Sjögreen, A stable FSI algorithm for light rigid bodies in compressible flow, *J. Comput. Phys.* 231 (17) (2013) 5854–5889.
- [11] C. Farhat, K. G. van der Zee, P. Geuzaine, Provably second-order time-accurate loosely-coupled solution algorithms for transient nonlinear computational aeroelasticity, *Computer Methods in Applied Mechanics and Engineering* 195 (17-18) (2006) 1973–2001.
- [12] M. Schäfer, M. Heck, S. Yigit, An implicit partitioned method for the numerical simulation of fluid-structure interaction, in: Bungartz, Schäfer (Eds.), *Fluid-Structure Interaction*, Springer, 2006, pp. 171–194.
- [13] J. Hron, S. Turek, A monolithic FEM/multigrid solver for an ALE formulation of fluid-structure interaction with applications in biomechanics, in: Bungartz, Schäfer (Eds.), *Fluid-Structure Interaction*, Springer, 2006, pp. 146–170.
- [14] T. E. Tezduyar, S. Sathe, Modelling of fluid-structure interactions with the space-time finite elements: Solution techniques, *International Journal for Numerical Methods in Fluids* 54 (6-8) (2007) 855–900.
- [15] I. Borazjani, L. Ge, F. Sotiropoulos, Curvilinear immersed boundary method for simulating fluid structure interaction with complex 3D rigid bodies, *J. Comput. Phys.* 227 (2008) 7587–7620.
- [16] J. Degroote, J. Vierendeels, Multi-solver algorithms for the partitioned simulation of fluid-structure interaction, *Computer Methods in Applied Mechanics and Engineering* 200 (25-28) (2011) 2195 – 2210.
- [17] J. T. Grétarsson, N. Kwatra, R. Fedkiw, Numerically stable fluid-structure interactions between compressible flow and solid structures, *J. Comput. Phys.* 230 (8) (2011) 3062 – 3084.
- [18] G. Hou, J. Wang, A. Layton, Numerical methods for fluid-structure interaction - a review, *Commun. Comput. Phys.* 12 (2012) 337–377.
- [19] G. Guidoboni, R. Glowinski, N. Cavallini, S. Čanić, Stable loosely-coupled-type algorithm for fluid-structure interaction in blood flow, *Journal of Computational Physics* 228 (18) (2009) 6916 – 6937.
- [20] S. Čanić, B. Muha, M. Bukač, Stability of the kinematically coupled β -scheme for fluid-structure interaction problems in hemodynamics, *ArXiv e-prints*.
- [21] F. Nobile, C. Vergara, An effective fluid-structure interaction formulation for vascular dynamics by generalized Robin conditions, *SIAM J. Sci. Comput.* 30 (2) (2008) 731–763.
- [22] C. A. Figueroa, I. E. Vignon-Clementel, K. E. Jansen, T. J. Hughes, C. A. Taylor, A coupled momentum method for modeling blood flow in three-dimensional deformable arteries, *Computer Methods in Applied Mechanics and Engineering* 195 (41-43) (2006) 5685 – 5706.
- [23] K.-J. Bathe, H. Zhang, Finite element developments for general fluid flows with structural interactions, *Int. J. Numer. Meth. Eng.* 60 (2004) 213–232.
- [24] M. Heil, An efficient solver for the fully coupled solution of large-displacement fluid-structure interaction problems, *Computer Methods in Applied Mechanics and Engineering* 193 (1–2) (2004) 1 – 23.
- [25] M. W. Gee, U. Küttler, W. A. Wall, Truly monolithic algebraic multigrid for fluid-structure interaction, *Int. J. Numer. Meth. Eng.* 85 (2011) 987–1016.

- [26] M. A. Fernández, J.-F. Gerbeau, C. Grandmont, A projection semi-implicit scheme for the coupling of an elastic structure with an incompressible fluid, *International Journal for Numerical Methods in Engineering* 69 (4) (2007) 794–821.
- [27] M. Astorino, F. Chouly, M. A. Fernández, Robin based semi-implicit coupling in fluid-structure interaction: Stability analysis and numerics, *SIAM J. Sci. Comput.* 31 (6) (2009) 4041–4065.
- [28] C. Conca, A. Osses, J. Planchard, Added mass and damping in fluid-structure interaction, *Computer Methods in Applied Mechanics and Engineering* 146 (3-4) (1997) 387 – 405.
- [29] P. L. Tallec, S. Mani, Numerical analysis of a linearised fluid-structure interaction problem, *Numerische Mathematik* 87 (2000) 317–354.
- [30] D. P. Mok, W. A. Wall, E. Ramm, Accelerated iterative substructuring schemes for instationary fluid structure interaction, in: K. Bathe (Ed.), *Computational Fluid and Solid Mechanics*, Elsevier, 2001, pp. 1325–1328.
- [31] C. Förster, W. A. Wall, E. Ramm, Artificial added mass instabilities in sequential staggered coupling of nonlinear structures and incompressible viscous flows, *Computer Methods in Applied Mechanics and Engineering* 196 (7) (2007) 1278 – 1293.
- [32] L. Gerardo-Giorda, F. Nobile, C. Vergara, Analysis and optimization of Robin-Robin partitioned procedures in fluid-structure interaction problems, *Siam J. Numer. Anal.* 48 (6) (2010) 2091–2116.
- [33] P. Causin, J. F. Gerbeau, F. Nobile, Added-mass effect in the design of partitioned algorithms for fluid-structure problems, *Comput. Method. Appl. Mech. Engrg.* 194 (2005) 4506–4527.
- [34] S. Badia, F. Nobile, C. Vergara, Robin-Robin preconditioned Krylov methods for fluid-structure interaction problems, *CMAME* 198 (33–36) (2009) 2768–2784.
- [35] F. Nobile, C. Vergara, Partitioned algorithms for fluid-structure interaction problems in haemodynamics, *Milan Journal of Mathematics* 80 (2) (2012) 443–467.
- [36] Y. Yu, H. Baek, G. E. Karniadakis, Generalized fictitious methods for fluid-structure interactions: Analysis and simulations, *Journal of Computational Physics* 245 (0) (2013) 317 – 346.
- [37] H. Baek, G. E. Karniadakis, A convergence study of a new partitioned fluid-structure interaction algorithm based on fictitious mass and damping, *Journal of Computational Physics* 231 (2) (2012) 629 – 652.
- [38] K. Riemsdlaugh, J. Vierendeels, E. Dick, An efficient coupling procedure for flexible wall fluid-structure interaction, in: *ECCOMAS Congress on Comp. Meth. in Appl. Sci. and Eng.*, Barcelona, 2000.
- [39] J. Degroote, A. Swillens, P. Bruggeman, R. Haelterman, P. Segers, J. Vierendeels, Simulation of fluid-structure interaction with the interface artificial compressibility method, *International Journal for Numerical Methods in Biomedical Engineering* 26 (3-4) (2010) 276–289.
- [40] P. Raback, J. Ruokolainen, M. Lyly, Fluid-structure interaction boundary conditions by artificial compressibility, in: *ECCOMAS Computational Fluid Dynamics Conference 2001 Swansea, Wales, UK*, 2001.
- [41] S. R. Idelsohn, F. Del Pin, R. Rossi, E. Oñate, Fluid-structure interaction problems with strong added-mass effect, *International Journal for Numerical Methods in Engineering* 80 (10) (2009) 1261–1294.
- [42] S. Badia, A. Quaini, A. Quarteroni, Splitting methods based on algebraic factorization for fluid-structure interaction, *SIAM J. Sci. Comput.* 30 (4) (2008) 1778–1805.
- [43] J. Degroote, P. Bruggeman, R. Haelterman, J. Vierendeels, Stability of a coupling technique for partitioned solvers in FSI applications, *Computers & Structures* 86 (23-24) (2008) 2224 – 2234.

- [44] J. Degroote, K.-J. Bathe, J. Vierendeels, Performance of a new partitioned procedure versus a monolithic procedure in fluid-structure interaction, *Computers & Structures* 87 (11-12) (2009) 793 – 801, Fifth MIT Conference on Computational Fluid and Solid Mechanics.
- [45] G. B. Whitham, *Linear and Nonlinear Waves*, John Wiley and Sons, New York, 1974.
- [46] J. J. H. Miller, On the location of zeros of certain classes of polynomials with applications to numerical analysis, *IMA J. Appl. Math.* 8 (3) (1971) 397–406.
- [47] J. C. Strikwerda, *Finite Difference Schemes and Partial Differential Equations*, Wadsworth and Brooks/Cole, 1989.
- [48] P. J. Roache, Code verification by the method of manufactured solutions, *ASME J. of Fluids Engineering* 124 (1) (2002) 4–10.
- [49] G. S. Chesshire, W. D. Henshaw, Composite overlapping meshes for the solution of partial differential equations, *J. Comput. Phys.* 90 (1) (1990) 1–64.